The Holographic Interface of a Fractional (2+1)D Topological Insulator at Finite Temperature

by

Anson W.C. Wong

B.Sc., The University of Waterloo, 2012

A THESIS SUBMITTED IN PARTIAL FULFILLMENT OF
THE REQUIREMENTS FOR THE DEGREE OF

MASTER OF SCIENCE

in

The Faculty of Graduate and Postdoctoral Studies

(Physics)

THE UNIVERSITY OF BRITISH COLUMBIA

(Vancouver)

October 2014

Abstract

Topological insulators are materials that are insulating in the bulk but conductive on the boundary. Although standard condensed matter techniques elucidate the dissipationless boundary physics of topological insulators well at weak coupling, they fail to do the same at strong coupling where exciting phenomena such as emergence and fractionalization are likely to occur. Fortunately the AdS/CFT correspondence offers an alternative perspective of the strong coupling limit in the form of a classical supergravity dual. In this thesis we realize the interface of a strongly-interacting fractional (2+1)D time-reversal invariant topological insulator at finite temperature by embedding a D5-brane with a $U(1)$ chemical potential into (AdS_5 black hole)$\times S^5$ supergravity. The thermodynamics of our interface are found to be considerably fermionic. Study of the interface has promising applications ranging from the design of spin channels in quantum computing, to the deeper understanding of highly-entangled systems.

Preface

This thesis is original and unpublished work of mine. An existing template for the implementation of spectral methods was provided by M. Rozali, but otherwise, I was responsible for all other analytical, numerical, and written aspects of this thesis. M. Rozali was my primary research advisor and was involved in the overall guidance and formulation of the project including the revisions of this thesis transcript. J. Karczmarek was the second reader of this thesis.

Table of Contents

Appendices

List of Tables

List of Figures

Acknowledgements

I thank first and foremost my parents for putting up with me throughout my whole life. Next up would be my caring aunts, uncles, and cousins that have taken care of me unconditionally – I am forever grateful. I thank all my closest friends from high school because I do not know where I would be in this world you guys were not around to help me transform from an immature little boy to a fully grown immature adult. I thank my former housemate James for all the funny, intellectual and emotional late-night conversations we have had during our ups and downs. I thank my storage room officemates Alex and Joel for making it much less lonely in our prison cell of an office, and the rest of the String Theory group for the fruitful physics discussions that I believe cannot possibly exist outside of the Hennings building. I thank Joanna for saying yes when I asked her to be my second reader for this thesis. And lastly, but most definitely not least, I thank my advisor Moshe for his constant guidance and patience throughout this project.

Dedication

To my lovely grandfather who sadly passed away during the writing of this thesis.

Chapter 1

Introduction

Holography is the study of how much information inside of a region of space is projected onto its own boundary. Often it is possible for the 'shadow' of an object to describe a lot, if not all, about the object itself. In string theory, the notion of holography is rooted in the physics of gravity and quantum mechanics. Take for example the Bekenstein-Hawking entropy of a black hole which is proportional to its event horizon area and not to its volume as classically expected [1]. The horizon here plays the role of the black hole's 'shadow' and tells a quantum story about the interior volume. First signs of a holographic principle coming to fruition in string theory originated from the work of 't Hooft and Susskind in the early 1990s [2, 3], but it was Maldecena in 1997 who provided an explicit hands-on example of how quantum mechanics could manifest itself as a hologram of gravity now infamously known as the AdS/CFT correspondence [4–8] (or gauge/gravity duality) which conjectures the equivalence between Type IIB string theory on $\mathrm{AdS}_5 \times S^5$ and $\mathcal{N} = 4$ super Yang-Mills theory in four dimensions. What is the practical use of the AdS/CFT duality though? The correspondence states the existence of a bijective mapping between the boundary fields of a gravity theory and the physical observables of its field theory dual. Although the specific mapping is not given freely to us a priori, with some work one can construct a holographic dictionary to infer the physics of a quantum field theory from an often simpler gravity calculation. Holography to this day remains as one of the forefronts of modern high energy physics research with applications in modelling high-temperature quark-gluon plasmas, computing holographic entanglement entropies, realizing confinement/deconfinement in non-abelian gauge theories, *etc.* Our intention in this thesis is to study the interface of a strongly-correlated topological insulator from a gravity point of view.

In condensed matter, majority of weakly-interacting systems follow the prescriptions of Fermi Liquid theory and/or Landau theory. These techniques however tend to fail when the interactions are more complicated: Fermi Liquid theory loses validity when the non-perturbative effects of strong coupling come into play, and Landau theory fails to track down novel phase

transitions in materials where the ordering mechanism is no longer an explicit breaking of symmetry *i.e* spin liquids. High-T_c superconductors and one-dimensional Luttinger liquids are examples of materials that are still poorly understood because of the lack of available techniques in field theory. Despite the current downfall of condensed matter at strong coupling, it is exactly at strong coupling where holography shines the brightest – a highly quantum system can be described by a gravity dual that is completely classical. At zero temperature, these are the scale-invariant systems that sit at the quantum critical point g_c for some physical running coupling g as illustrated in Fig 1.1. As the temperature increases, the quantum critical point extends into the quantum critical phase. A plethora of strongly-correlated versions of high-T_c superconductivity [9], the Josephson effect [10], the Kondo effect [11], non-Fermi liquids [12, 13], the integer/fractional quantum Hall effect [14–16], and striped phases [17] have been holographically realized in this phase already to name a few. Although holographic techniques in condensed matter are somewhat contrived because they demand the strict conditions of supersymmetry and a large number of colours, they do on the very up side serve as promising indicators for universal behaviour in the strong coupling regime – currently we have no simpler alternative.

We are interested in applying holography to topological insulators [18–22]. Topological insulators are insulators that are gapped in the bulk but gapless on the boundary, as opposed to conventional insulators where it is gapped in both places. Moreover the admitted gapless boundary states of a topological insulator are protected by bulk symmetries (typically time-reversal invariance) from dissipative processes like electron-impurity scattering. A convenient mental picture of the topological insulator is a conventional insulator with a thin coating of metal, but the reality is that the topological insulator is uniform throughout.

The peculiar behaviour of the boundary of a topological insulator comes as a consequence of topology. Insulators of differing topological classes coming in contact with one another necessarily forms a gapless interface for fermionic transport. In this thesis we study in particular the interface of a (2+1)D time-reversal invariant topological insulator at finite temperature. The topological invariant is well known to be $\mathbb{Z}_2$-valued at weak coupling. At strong coupling, it has been proposed that the fermions in the bulk of the topological insulator can fractionalize into partons [23, 24]. We holographically realize this fractional topological insulator by using a top-down approach of embedding a probe D5-brane with a $U(1)$ chemical potential into an (AdS_5 black hole) $\times$ S^5 background similar to what was done in Refs [25–27]. The interface is localized by placing two different topologi-

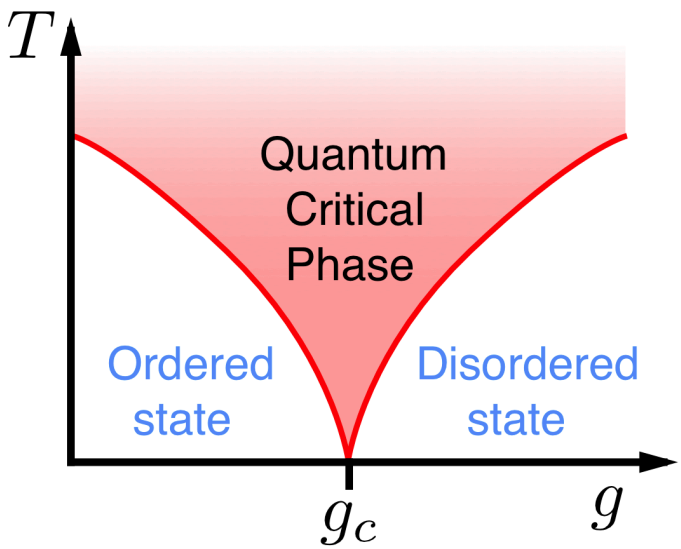

Figure 1.1: The quantum critical point g_c and quantum critical phase (sandwiched between the ordered and disordered state) as a function of temperature T and running coupling g. In the quantum critical phase, the theory is independent of length scale.

cal phases in contact with eachother via flipping the fermionic mass sign along some spatial direction. We then construct a phase diagram and study the thermodynamics of a representative interface solution. The (3+1) dimensional version of our problem was investigated in Refs [28, 29] but it remained to be done in (2+1) dimensions until now. Sanity checks of our numerical calculations were made and found to agree with the relevant results of Refs [25, 28–32].

The thesis will be structured as follows. We introduce the AdS/CFT correspondence in Chapter 2. Afterwards, we stray from string theory for a while and introduce the topological insulators in Chapter 3. In Chapter 4, we construct step-by-step the holographic interface of a fractional (2+1)D time-reversal invariant topological insulator. The numerical results are presented and discussed in Chapter 5. We conclude in Chapter 6 and provide prospective research in Chapter 7.

Chapter 2

The AdS/CFT correspondence

We briefly introduce the AdS/CFT correspondence conjecture with D-branes and its use towards studying strongly coupled systems. The AdS/CFT correspondence states the duality:

Field theory side		**Gravity side**
$\mathcal{N}=4$ super Yang-Mills theory $SU(N_c)$ in (3+1) dimensions	$\Leftrightarrow$	Type IIB superstring theory on $\mathrm{AdS}_5 \times S^5$ spacetime
Gauge-invariant operators	$\leftrightarrow$	Supergravity fields on the boundary

On the field theory side of the correspondence, $\mathcal{N}=4$ super Yang-Mills theory is a conformal non-abelian gauge theory with a vanishing β function (at all perturbative orders) and is maximally supersymmetric. The quarks of the theory transform in the fundamental representation of the special unitary $SU(N_c)$ gauge group with N_c being the number of quark colours. The field content of the theory includes a gauge field, four Weyl spinors, and six scalars. There are $4\mathcal{N}=16$ supercharges due to each of the four Weyl spinors holding two complex degrees of freedom. The combination of the $SO(4,2)$ Lorentzian conformal group and the $SO(6)$ R-symmetry between the six scalars gives for an $SO(4,2)\times SO(6)$ symmetry group.

On the gravity side of the correspondence, Type IIB string theory is on a maximally symmetric spacetime of 5-dimensional Anti-de Sitter (AdS) space producted with a 5-dimensional sphere S^5. AdS space naturally exhibits the conformal invariance of the field theory with an 'extra' radial variable z that adjusts the lattice renormalization length so that the physics are independent of length-scale. The isometries of AdS_5 and S^5 producted together give for the same $SO(4,2)\times SO(6)$ symmetry as it is on the field theory side. Performing a dimensional reduction of the compact S^5 sphere makes

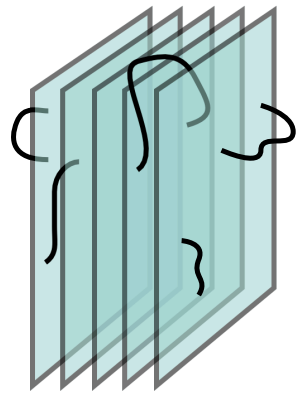

Figure 2.1: A stack of coincident D3-branes with open strings connecting the brane with either itself or another identical brane to enhance the gauge group to $SU(N_c)$. Gauge fields are sourced at the end-points of the connected strings.

the gravity side effectively a (4+1)-dimensional AdS gravity theory with an infinite number of fields – one dimension higher than the (3+1)-dimensional field theory 'hologram'.

2.1 AdS/CFT from D3-branes

Dp-branes are solitonic hyperplanes in string theory that extend in one temporal direction and p spatial directions [33–35]. They provide world volume surfaces for open strings to attach their ends onto to source Ramond-Ramond gauge fields at the string ends so that scalars, vectors, and fermions can live on them as dynamical degrees of freedom. Neumann boundary conditions are satisfied in $(p+1)$ of the transverse directions of the brane, and Dirichlet conditions are satisfied in the remaining $10-(p+1)$ orthogonal directions. The gauge/gravity conjecture can come about by considering extremal D3-branes from two different perspectives: the open string perspective as a stack of coincident D3-branes connected by open strings, and the closed string perspective as a black 3-brane gravity solution.

The open-string persective

The coincident N_c D3-brane stack in the open-string perspective, as depicted in Figure 2.1, has an action of the form

$$S^{\mathbf{FT}} = S^{\mathbf{FT}}_{\text{D3-brane}} + S^{\mathbf{FT}}_{\text{bulk}} + S^{\mathbf{FT}}_{\text{int}}, \tag{2.1}$$

which is comprised of the action of the D3-branes, the bulk they sit in, and the interactions between them. In the Maldecena decoupling limit of vanishing string tension $\alpha' \to 0$, the interaction part $S^{\mathbf{FT}}_{\text{int}} \to 0$ vanishes and the D3-brane stack becomes $\mathcal{N} = 4$ super Yang-Mills theory with an $SU(N_c)$ colour symmetry embedded in flat space

$$S^{\mathbf{FT}} \underset{\alpha' \to 0}{=} S^{\mathbf{FT}}_{\mathcal{N}=4 \text{ Yang-Mills}} + S^{\mathbf{FT}}_{\text{flat-space}}. \tag{2.2}$$

The closed-string persective

Now consider the same D3-brane stack but in the closed-string perspective of an extremal black 3-brane solution. The black 3-brane metric is given by

$$ds^2_{\text{D3}} = H(r)^{-\frac{1}{2}} \left(-dt^2 + d\vec{x}^2\right) + H(r)^{\frac{1}{2}} \left(dr^2 + r^2 d\Omega_5^2\right), \tag{2.3}$$

where $H(r) = 1 + L^4/r^4$ is the warp factor, r is the radial parameter, $L^4 = 4\pi g_s N_c \alpha'^2$ is the AdS length, and $d\Omega_5^2$ is the 5-sphere metric. The near-horizon limit $H(r \ll L) \approx L^4/r^4$ corresponds to $\text{AdS}_5 \times S^5$ geometry, and the boundary limit $H(r \gg L) \approx 1$ corresponds to flat $\mathbb{R}^{1,9}$ Minkowski space as illustrated in Fig 2.2. Taking the Maldecena decoupling limit decouples the near-horizon and the boundary geometries of the curved background and leaves the action as

$$S^{\mathbf{G}} \underset{\alpha' \to 0}{=} S^{\mathbf{G}}_{\text{AdS}_5 \times S^5} + S^{\mathbf{G}}_{\text{flat-space}}. \tag{2.4}$$

Equating the actions from the open and closed string perspectives and subtracting the shared flat space component leaves us with the perturbative intuition that $\mathcal{N} = 4$ $SU(N_c)$ super Yang-Mills theory is dual to Type IIB string theory on $\text{AdS}_5 \times S^5$ in the large $N_c \sim 1/\alpha' \to \infty$ limit for arbitrary coupling strength $\lambda \equiv g^2_{\text{YM}} N_c = 2\pi g_s N_c$ (g_{YM} and g_s being the Yang-Mills and string couplings respectively) .

2.2 The strong coupling limit

The large $N_c \sim 1/\alpha' \to \infty$ limit with λ fixed, also known as the planar limit, provides integrability by suppressing the $1/N_c^{2g}$ contributions from non-planar genus $g > 0$ Feynman diagrams to give precedence to only the planar $g = 0$ diagrams. Although the strings are free in the $\alpha' \to 0$ limit,

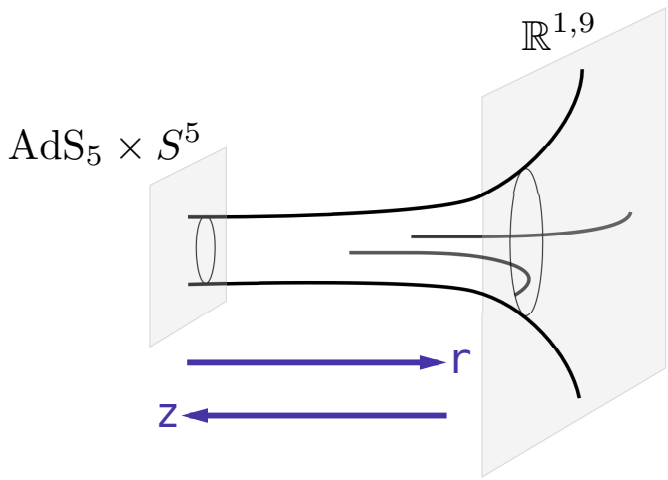

Figure 2.2: The D3-brane stack as a black 3-brane. The geometry is $\mathrm{AdS}_5 \times S^5$ near the horizon, and $\mathbb{R}^{1,9}$ Minkowski near infinity. The compactified S^5 manifold gives a minimum size to the 'throat' of the near-horizon brane geometry.

they are still quantum-like and can form massive towers of string modes that correspond to higher-order curvature terms in the gravity action. However, if we take an additional strong coupling $\lambda \to \infty$ limit as well, such stringy effects get suppressed and the strings become not only free but classical as illustrated in Fig 2.3. This is the beauty of the strong coupling limit in AdS/CFT. Validity of perturbation theory on the field theory side holds only at weak-coupling

$$\lambda = g_{\mathrm{YM}}^2 N_c \ll 1, \tag{2.5}$$

whereas the perturbative validity on the gravity side (for string length l_s) holds only at strong coupling

$$\lambda = g_s N_c \sim L^4/l_s^4 \gg 1, \tag{2.6}$$

making the perturbative physics on one side of the duality resemble the non-perturbative physics on the other side. We will make use of both the large $N_c \to \infty$ and strong coupling $\lambda \to \infty$ limits in our holographic set-up.

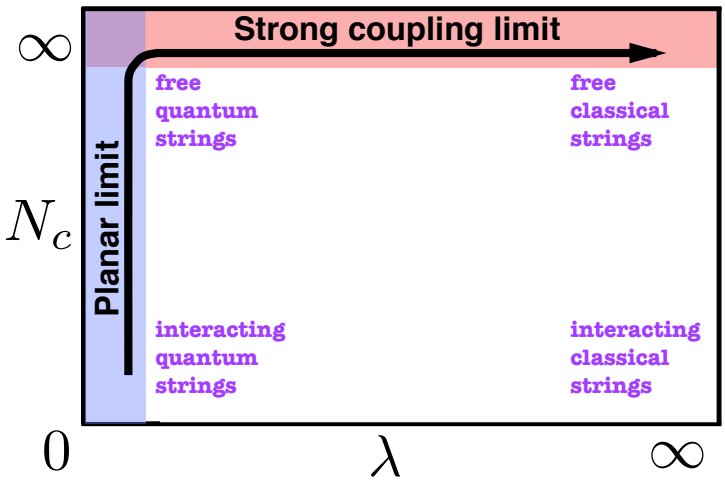

Figure 2.3: We take the large N_c limit before we take the strong coupling $\lambda \to \infty$ limit to achieve a classical gravity dual. The planar limit frees the strings and the strong coupling limit allows for classical treatment.

2.3 Finite temperature AdS/CFT

The use of extremal D3-branes in the AdS/CFT duality keeps the physics pertinent to only zero temperature. Holography at finite temperature involves adding thermal excitations to the AdS space to get 'hot' AdS – this corresponds to a thermal bath in the dual field theory. By replacing the extremal D3-branes with non-extremal ones we move out to finite temperature. The near-horizon geometry of the D3-branes changes from $\mathrm{AdS}_5 \times S^5$ to (AdS_5 black hole) $\times S^5$ with a radial horizon proportional to the field theory temperature. Overall the promotion to finite temperature changes the gravity side of the correspondence to Type IIB string theory on (AdS_5 black hole)$\times S^5$. Note that the boundary geometry is unchanged from replacing the D3-branes; the horizon of the black hole effectively cuts off all infrared physics below temperature T but leaves the ultraviolet physics at the AdS boundary unscathed. We work with finite temperature exclusively in this thesis.

Chapter 3

Topological insulators

Quantum mechanics is responsible for the inert behaviour of conventional insulators. At sufficiently low temperatures, the valence electrons cannot overcome the energy threshold of $\Delta > 0$ to climb up into the conduction band. The band structure diagram for electrons in a conventional insulator is illustrated in Fig 3.1a with both the bulk and boundary being gapped. Such insulators are rather dull and luckily represent only a subset of materials with gapped bulks. We focus here on another class of insulators called the topological insulators.

Topological insulators fit somewhere between an insulator and a conductor in the sense that it has a gapped bulk but a gapless boundary. The boundary can conduct fermions even in the presence of an insulating bulk. In non-interacting models, the (2+1)D topological insulator has been exhaustively classified in a periodic table of discrete symmetry classes in the bulk that includes time-reversal symmetry, charge conjugation symmetry, and sublattice symmetry [36, 37]. The most studied example is the (2+1)D time-reversal invariant quantum spin Hall (QSH) state and unlike most discoveries in condensed matter, the prediction of their existence well preceded its experimental realization by almost 20 years when it was first observed in two-dimensional HgTe quantum wells in 2007 [38, 39]. QSH states are time-reversal invariant in the bulk and can exhibit the QSH effect of spin-locked electronic transport along the insulator edge analogous to Hall current in the quantum Hall effect. We illustrate both the QSH effect and quantum Hall effect in Fig 3.2b and Fig 3.2c, and their corresponding band structure diagrams in Fig 3.1b and Fig 3.1c. The spin-orbit coupling from lattice electrons induce a magnetic-like field to drive Kramers pairs of opposite-spin fermions to counter-propagate on the edge of the QSH state [40, 41], whereas the external magnetic field in the quantum Hall effect breaks time-reversal symmetry and forces mixed-spins to propagate along the edge in the same direction.

The edge of the QSH state, topologically speaking, is simply the shared interface between a trivial conventional insulator (like vacuum) and a non-trivial topological insulator. We want to holographically construct such an

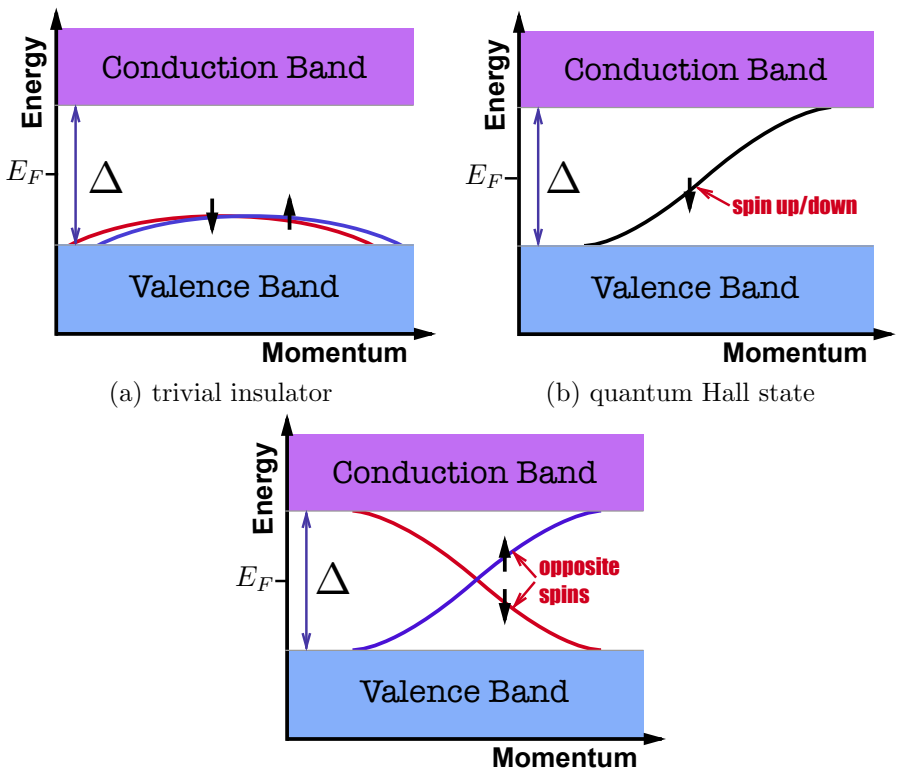

(a) trivial insulator

(b) quantum Hall state

(c) QSH state

Figure 3.1: The band structure diagrams for different (2+1)D insulators. The bulk is gapped and non-conducting for each insulator above. The trivial insulator is completely gapped in both the bulk and the boundary. The boundary for the quantum Hall and QSH states are gapless and can thus support boundary transport. The Hall current travels in one direction with no spin dependence, but the QSH current has two counter-propagating channels of opposite spins.

interface for the (2+1)D time-reversal invariant topological insulator. To do so, we begin by discussing the possible topological phases that can exist in our insulator.

3.1 The $\mathbb{Z}_2$ phases

Symmetry brings about the concept of topology to insulators. In mathematics, the topology of a geometrical object is characterized by its topological invariant – an intrinsic quantity that is insensitive to smooth deformations of the object. A sphere is topologically equivalent to an ellipsoid but not to a torus without the use of scissors. Analogously in non-interacting topological insulators, the dispersion spectra of topologically distinct insulators are not smoothly connected from one to another without closing the bulk gap (take for example the band structure diagrams of the trivial and non-trivial insulators in Fig 3.1a and Fig 3.1c). Topology in general is not restricted to insulators – superconductors can be topological as well because of a gapped bulk from Cooper pairing, but gapless materials such as metals and doped semi-conductors cannot be given such a classification.

The topological invariant of a topological insulator is encoded in the anomalous Chern-Simons terms that come from integrating out massive fermions from the action. For the (2+1)D time-reversal invariant topological insulator, the bulk topological invariant is $\mathbb{Z}_2$-valued meaning only two distinct topological classes exist and they happen to be the trivial (conventional) insulator and the non-trivial (topological) insulator. The even/odd parity of the number of edge pair modes N_f crossing through the Fermi energy E_F identifies the $\mathbb{Z}_2$ phases – an odd N_f being of the same class as the trivial insulator, and an even N_f being of the same class as the non-trivial insulator.

Another way of identifying the $\mathbb{Z}_2$ invariant of the QSH state is through the mass sign of the bulk fermions. Consider the microscopic (2+1)D time-reversal invariant model for a single $N_f = 1$ flavour pair of free complex Dirac fermions ψ_1 and ψ_2 in spinor notation

$$\mathcal{L} = \bar{\psi}_1 \left(i\gamma^\mu \partial_\mu + m\right) \psi_1 + \bar{\psi}_2 \left(i\gamma^\mu \partial_\mu - m\right) \psi_2, \tag{3.1}$$

with oppositely signed masses $\pm m$, a Dirac conjugate $\bar{\psi} \equiv \psi^\dagger \sigma^z$, and gamma matrices γ^μ made of Pauli matrices σ^i. Let us inspect the mass terms $\pm m$. They are necessarily real by time-reversal invariance. Although the $\pm m\bar{\psi}\psi$ terms are not time-reversal invariant individually because

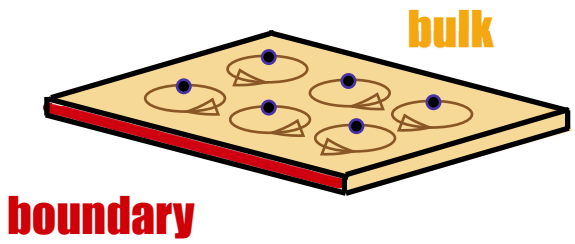

(a) trivial insulator

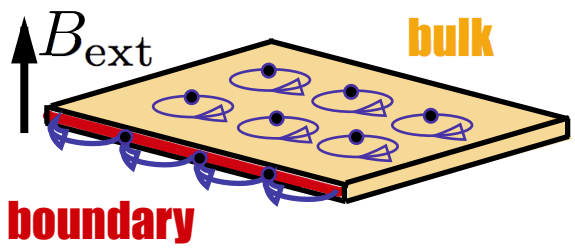

(b) quantum Hall state

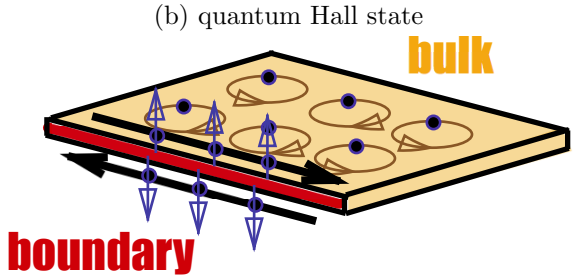

(c) QSH state

Figure 3.2: Schematic diagrams of the conduction (or non-conduction) of edge states in different (2+1)D insulators. The trivial insulator in Fig 3.2a is fully gapped at the boundary and supports zero conductivity. The quantum Hall state in Fig 3.2b conducts Hall current on the edge given a strong external magnetic field B_{ext}. The spin current on the edge of a QSH state as shown in Fig 3.2c comes as Kramers doublets of opposite spin electrons traveling in opposite directions. Spin-orbit coupling drives spin transportation in the QSH effect. Unlike (3+1)D, the boundary states are restricted to only two directions of travel along the edge of a (2+1)D insulator. Note that QSH states have no net electric charge flowing along the edge.

$T\bar{\psi}\psi T^{-1} = -\bar{\psi}\psi$ is parity odd, the combination of them together is. Time-reversal symmetry forces the fermions to exist as degenerate Kramers pairs with oppositely-signed masses and spin. At the edge where the fermionic modes are massless $m = 0$, the theory exhibits a global $U(1)\times SU(2N_f)$ symmetry. This $SU(2N_f) \doteq SU(2)$ symmetry allows for the massless fermions to transform non-trivially from one another under the non-abelian flavour group. In the bulk where the mass is finite $m \neq 0$ (this could be negative or positive), the global symmetry breaks down to $U(N_f) \times U(N_f) \doteq U(1) \times U(1)$. These two $U(1)$ groups represent Maxwell electromagnetism and R-symmetry in supersymmetric gauge theories. Moreover, under the lexicon of condensed matter, the R-symmetry represents the conservation of the z-component of spin. All fermions in this model carry the same $U(1)$ Maxwell charge of $q^{\text{Maxwell}} = +1$, but as for the $U(1)$ R-charges, only half of them carry $q^R = +1$ with the remaining half carrying $q^R = -1$.

The classical description of our massive (2+1)D fermionic model is chirally invariant to axial rotations ϕ. At the quantum level though, chirality is no longer a symmetry and the massive theory develops an anomalous quadratic $A^R \wedge dA^{\text{Maxwell}}$ Chern-Simons term [19] of level

$$k \;=\; \frac{1}{2}\sum_i q_i^{\text{Maxwell}} q_i^R \,\text{sgn}(m_i) \;=\; \text{sgn}(m)N_f \;\doteq\; \text{sgn}(m) \tag{3.2}$$

from integrating out the $N_f = 1$ massive fermion pair, where A^R and A^{Maxwell} are the $U(1)$ R and Maxwell gauge fields respectively, and the index i runs through all fermionic fields. A quick summary of this Chern-Simons term can be found in Appendix A. What is important is that the topological invariant $k = \text{sgn}(m) = \pm 1$ is exactly the discrete $\mathbb{Z}_2$-valued topological invariant we were expecting. The result of having the mass sign fully determine the topological phase is in agreement with what is allowed of the chiral rotation parameter ϕ: only $\phi = 0$ and $\phi = \pi$ rotations are permitted by time-reversal symmetry and these anomalously rotate the mass by $\exp(-i\phi)|_{\phi=0,\pi}$ to give the same $m = \pm M$ classification.[1] For the remainder of this thesis, we will label the $m > 0$ phase as the trivial insulator, and the $m < 0$ phase as the non-trivial insulator without any loss of generality.

[1] Time-reversal symmetry demands $\phi = -\phi \pmod{2\pi}$ to be satisfied.

3.2 The strong coupling limit and fractionalization

What is less understood, but much more interesting, is the case when fermionic interactions are turned on. One naturally relates back to the non-interacting case and asks questions like: Do the same topological phases hold? If not, what do they become? How do strong correlations affect the edge physics? For the (2+1)D time-reversal invariant topological insulator, it has been proposed that the electrons inside of the bulk of the non-trivial insulator fractionalize into partons at large N_c and strong coupling [23, 24]. Implementing fractionalization involves breaking up each fermion into N_c partonic fragments with each piece holding a $1/N_c$ fraction of the R and Maxwell charge of the fermion which for $N_f = 1$ gives an $A^R \wedge dA^{\text{Maxwell}}$ Chern-Simons term of level

$$k_{\text{frac}} \;=\; \frac{1}{2}\sum_i q^{\text{Maxwell}}_{\text{frac},i} q^R_{\text{frac},i}\ \text{sgn}(m_i) \;=\; \frac{\text{sgn}(m)N_f}{N_c} \;\doteq\; \frac{\text{sgn}(m)}{N_c}. \tag{3.3}$$

This is the fractionalized version of our integral Chern-Simons term from (3.2); it takes the integral topological invariant $k = \pm 1$ and divides it by N_c. Note that the fractional topological invariant is still $\mathbb{Z}_2$-valued and dependent on the mass sign – an interface will still be localized from a discontinuous flip of the fermionic mass sign. The partons outside of the bulk of the non-trivial insulator are confined, but inside the bulk, the large N_c limit of the $SU(N_c)$ gauge group adds in light matter that can drive the partons to deconfine [28, 42]. Our holographic description of the topological insulator incorporates fractionalization naturally because AdS/CFT extensively utilizes both the large N_c and large λ limits. In the next chapter we will discuss how the corresponding Wess-Zumino terms on the gravity side matches exactly with this fractionalized Chern-Simons term.

3.3 A topological interface

To deform from one topological phase to the other, the sign of the mass must flip regardless of whether the insulator is fractional or not. This necessarily localizes gapless modes simply by interpolation. If we put a trivial insulator in contact with a non-trivial insulator at some spatial slice $x = x_{\text{int}}$, the shared interface will be gapless and localized at $x = x_{\text{int}}$; for if the interface gap did not close, it would suggest that the two insulators in contact were

not of different topological classes to start off with. Spatially varying the real mass profile of a fermion $m(x)$ so that it discontinuously switches signs at $x = x_{\text{int}}$ will do what we wish for. On the gravity side, this will correspond to the passing of a D5-brane through a D3-brane stack.

Chapter 4

Gravity side set-up

We construct the gravity dual of the static interface of a (2+1)D holographic topological insulator infixed in a (3+1)D $\mathcal{N} = 4$ super Yang-Mills theory by embedding a D5-brane into (AdS_5 black hole) $\times S^5$ using the ideologies of Chapters 2 and 3. Our D5-brane embedding follows closely the embeddings explored in Refs [25, 26], and it was shown in Refs [26, 43] that our set-up does in fact fractionalize the bulk fermions at large N_c and large λ. From Ref [26], the relevant Wess-Zumino term

$$S_{\mathrm{WZ}} = \frac{N_c N_f}{4\pi} \int d^2x \int dt \left(A^R \wedge F + A \wedge F^R \right) \tag{4.1}$$

has a coefficient that is equal to the level of the fractionalized Chern-Simons term $k_{\mathrm{frac}} = N_c N_f$ divided by 4π (in their notation[2]). The exact matching of the anomalous terms on both sides of the duality suggests the naturalness of fermions to fractionalize in holographic topological insulators. As the anomalous terms are independent of the details of the D5-brane embedding, what remains is the construction of an interface that can support the QSH effect by spatially varying a fermionic mass profile $m(x)$ so that it has a root at some spatial slice $x = x_{\mathrm{int}}$. Additionally, we feed in a homogenous chemical potential μ to the system via a $U(1)$ Maxwell gauge field on the D5-brane.

4.1 The field theory to realize

$\mathcal{N} = 4$ super Yang-Mills theory with a non-abelian $SU(N_c)$ gauge group will serve as an appropriate (3+1)D background field for us to add our defect fermions into. As discussed in Chapter 2, an N_c stack of coincident D3-branes will actualize this background. Although the statistical $SU(N_c)$ gauge fields are gapless, they do not contribute to electronic transport because they are electrically neutral – they act as the thermodynamic gauge

[2]The notation of Ref [26] has $k_{\mathrm{frac}} = N_c N_f$ from defining the charge of the fermion to be N_c so that each parton holds a charge of magnitude one (instead of $1/N_c$).

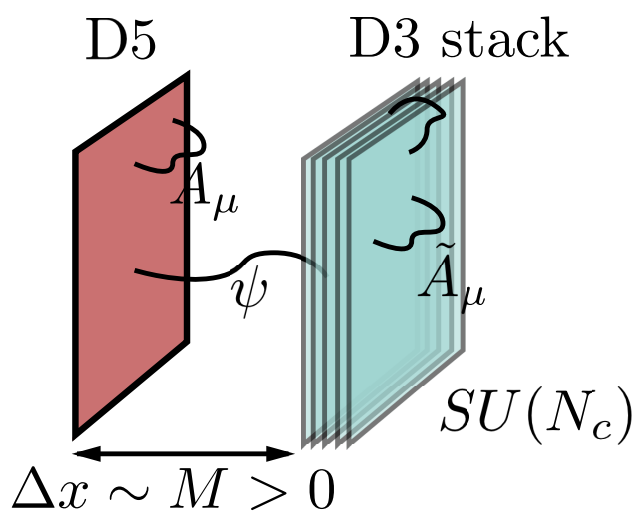

Figure 4.1: The D3-D5 brane system for a single $N_f = 1$ D5 probe brane. The A_μ on the D5-brane is a global $U(N_f) \doteq U(1)$ gauge field, and the $\tilde{A}_\mu$ on the D3-brane stack is an internal $SU(N_c)$ 'phonon' gauge field. The string connecting the D3 and D5 branes is the Dirac fermion ψ. Separating the D5-brane from the D3-branes gives mass to the fermion.

'phonons' that make up the insulator. Conformal symmetry at large N_c pushes the phonons to deconfine our partons [44].

Adding N_f D5 flavour branes to the D3-brane stack yields N_f pairs of fermions that are restricted to propagate on a (2+1)D hypersurface of the (3+1)D field theory in addition to the original $\mathcal{N} = 4$ field content [45–47]. The (2+1)D defect comes from the D5-branes omitting one of the flat directions occupied by the D3-brane stack. Adding in N_f D5-branes couples N_f $\mathcal{N} = 2$ fundamental hypermultiplets to $\mathcal{N} = 4$ super Yang-Mills theory which halves the original number of supersymmetries. Extra scalars are inevitably added to the field content as part of introducing the $\mathcal{N} = 2$ hypermultiplet but they can be safely ignored because of their non-contribution to the anomalous physics [26]. We illustrate our D3-D5 brane picture for $N_f = 1$ in Fig 4.1. The defect Dirac fermion is the string between the D3 and D5 branes and it has a generated mass proportional to the spatial separation of the branes.

We localize the zero modes by considering the supersymmetric D3-D5 brane intersection. This is illustrated in Fig 4.2 as a D5-brane passing through the D3-brane stack. Prior to the decoupling limit, both branes occupy directions in the world volume as tabulated in Table 4.1. There is

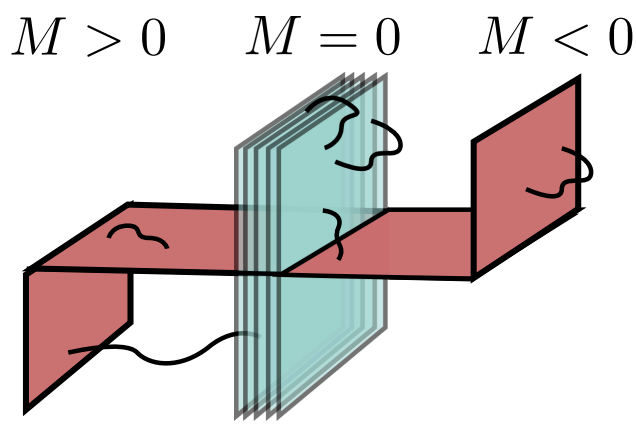

Figure 4.2: The supersymmetric D3-D5 brane intersection. By passing the D5-brane through the D3-brane stack in the transverse x_9 direction, the mass of the fermion can switch signs to realize a gapless interface. Positive and negative mass embeddings correspond to which side of the D3-brane stack the D5-brane is being pulled away from.

Poincaré invariance in the 012 directions and $SO(3)$ rotational symmetry in the 456 directions of the D5-brane. Pulling the D5-brane away from the D3-brane stack in a common transverse direction, say x_9, gives mass to the hypermultiplet by reducing the $SO(3)$ symmetry to $SO(2) \approx U(1)$ in the transverse 789 directions of both branes. After taking both the decoupling and strong coupling limits at finite temperature, the holographic picture greatly simplifies to N_f D5-branes being embedded into (AdS_5 black hole) $\times$ S^5 geometry. Furthermore the gravitational backreaction of the D5-brane on the metric $g_{\mu\nu}$ can be neglected because of an N_f/N_c quenching of quark loop corrections in the stress energy tensor $T_{\mu\nu}$ [48, 49]. Therefore our D5-branes can be treated as probe branes in a fixed supergravity background.

	x_0	x_1	x_2	x_3	x_4	x_5	x_6	x_7	x_8	x_9
D3 (background):	•	•	•	•	○	○	○	○	○	○
D5 (probe):	•	•	•	○	•	•	•	○	○	○

Table 4.1: Directions occupied by the branes in our D3-D5 system. The filled circles • represent the directions occupied by the brane, and the unfilled circles ○ represent the orthogonal directions unoccupied by the brane in the world volume. The D5-brane probes the D3-brane stack background.

4.2 The D5-brane embedding

Our D5-brane embedding occupies 6 directions of the possible 10 directions of (AdS_5 black hole) $\times S^5$. The embedding extends along a 4-dimensional slice of the 5-dimensional AdS_5 black hole by neglecting one of the three spatial directions, and wraps an S^2 around the S^5.

The metric

We write the (AdS_5 black hole) $\times S^5$ metric $g_{\mu\nu}$ as

$$ds^2 = \frac{r^2}{L^2}\left[-f(r)dt^2 + d\vec{x}_3^2\right] + \frac{L^2}{r^2}\left[\frac{dr^2}{f(r)} + r^2 d\Omega_5^2\right], \tag{4.2}$$

$$d\vec{x}_3^2 = dx^2 + dy^2 + dz^2, \tag{4.3}$$

$$d\Omega_5^2 = d\theta^2 + \cos^2\theta d\hat{\Omega}_2^2 + \sin^2\theta d\Omega_2^2, \tag{4.4}$$

$$f(r) = 1 - \frac{r_h^4}{r^4}, \tag{4.5}$$

where r_h is the radial horizon of the AdS_5 black hole, $d\vec{x}_3^2$ is the metric for 3-dimensional Euclidean space, and $d\Omega_m^2$ is the metric for the m-sphere S^m. The first half of the metric is the AdS_5 black hole written in global coordinates (t, x, y, z, r) with an AdS length of L, and the remaining half is a 5-sphere of radius L. One can convert from these coordinates to isotropic coordinates with a $\rho^2 = r^2 + \sqrt{r^4 - r_h^4}$ transformation; this convention is used extensively in Refs [50, 51] for the D3-D7 system and it gives a metric of the form

$$ds^2 = \frac{1}{2}\frac{\rho^2}{L^2}\left[-\frac{f(\rho)^2}{h(\rho)}dt^2 + h(\rho)d\vec{x}_3^2\right] + \frac{L^2}{\rho^2}\left[d\rho^2 + \rho^2 d\Omega_5^2\right], \tag{4.6}$$

$$f(\rho) = 1 - \frac{r_h^4}{\rho^4}, \tag{4.7}$$

$$h(\rho) = 1 + \frac{r_h^4}{\rho^4}. \tag{4.8}$$

Assuming thermal equilibrium, the gauge theory temperature T can be identified as the Hawking temperature through the elimination of the conical singularity at the horizon. Euclideanizing the metric with a $\tau = it$

Wick rotation sets the inverse temperature β to be τ-periodic, which in turn gives a Hawking temperature of $T = \beta^{-1} = r_h/(\pi L^2)$. The details of this calculation can be found in Appendix B.

The embedding

We choose our 5-sphere metric parameterization to be

$$d\Omega_5^2 = d\theta^2 + \cos^2\theta d\hat{\Omega}_2^2 + \sin^2\theta d\Omega_2^2, \tag{4.9}$$

for the convenience of wrapping an S^2 around the S^5 where $d\Omega_2^2 = d\psi^2 + \sin^2\psi d\phi^2$ is the S^2 metric with the hat indicating which of two 2-spheres is the one being embedded. The parameter $\theta \in \left[-\frac{\pi}{2}, \frac{\pi}{2}\right]$ here controls the S^2 'slipping' mode around the S^5.

With the full metric (4.2) in hand, the D5-brane embedding in terms of the 10 world sheet coordinates X^μ can be catalogued as

$$X^\mu = (t, r, x, y, z, \theta(r,x), \psi_1, \psi_2, \phi_1, \phi_2)\,, \tag{4.10}$$

where $\theta \equiv \theta(r,x)$ is our embedding parameter from metric (4.9). For our purposes it is only dependent on the the radial coordinate r and the spatial coordinate x because of Poincaré invariance and rotational symmetry. Additionally we set up a Maxwell $U(1)$ gauge field A_μ to live on the world volume of the D5 brane as

$$A_\mu = (A_t(r,x), \vec{0}), \tag{4.11}$$

with the only non-vanishing component being the temporal one. Including non-vanishing spatial components A_i into the gauge potential breaks time-reversal invariance in the action [52]. The gauge field $A_t \equiv A_t(r,x)$ too depends only on r and x by symmetry. Our D5-brane has 6 embedding coordinates

$$\xi^a = (t, r, x, y, \psi_1, \phi_1)\,, \tag{4.12}$$

which give for an induced metric on the D5-brane (with $L = 1$ set to make use of conformal symmetry) of

$$\begin{aligned} ds_{\mathrm{D5}}^2 &= r^2\left[-f(r)dt^2 + \left(1 + \frac{(\partial_x\theta)^2}{r^2}\right)dx^2 + dy^2\right] + 2(\partial_r\theta)(\partial_x\theta)drdx \\ &\quad + \left(\frac{1}{r^2 f(r)} + (\partial_r\theta)^2\right)dr^2 + \cos^2\theta\left(d\psi_1^2 + \sin^2\psi_1 d\phi_1^2\right). \end{aligned} \tag{4.13}$$

Moving the D5-brane through the D3-brane stack in a common transverse direction to switch mass signs is implicitly controlled by the embedding parameter θ. Later on we will see that the mass profile is actually related to the asymptotic expansion of the embedding function by $\theta(r \to \infty, x) \approx \frac{m(x)}{r}$.

4.3 DBI action and equations of motion

Given the embedding in terms of the $\{\theta, A_t\}$ bulk fields, we now proceed on with finding the brane action and its associated equations of motion. An appropriate action to use for the brane embedding in the decoupling limit is the Dirac-Born-Infeld (DBI) action. It generalizes the Nambu-Goto action and recovers the Yang-Mills action in the weak α' expansion. The DBI action contains two types of D-brane excitations: the external rigid isometries and deformations of the brane geometry, and the internal world volume gauge fields sourced by open string ends. In general, the DBI action for N_f decoupled D5-branes takes the form

$$S_{\mathrm{D5}} = -\frac{N_f T_{\mathrm{D5}}}{g_s} \int d^6\xi \sqrt{-\det\left(\gamma_{ab} + 2\pi\alpha' F_{ab}\right)}, \tag{4.14}$$

where γ_{ab} is the induced (or pullback) metric (4.13) on the D5-brane defined by $\gamma_{ab} \equiv \frac{\partial X^\mu}{\partial \xi^a}\frac{\partial X^\nu}{\partial \xi^b} g_{\mu\nu}$ with ξ^a being the embedding coordinates from (4.12), F_{ab} is the pullback of the field tensor living on the world volume of the D5-brane, and T_{D5} is the tension of the D5 brane. The latin indices a, b run over the 6 embedding coordinates. The determinant inside of the square root is responsible for mixing the tensor terms together to make for non-trivial interaction dynamics.

With a re-parameterization of the embedding field $\chi \equiv \chi(r, x) = \sin\theta(r, x)$ and a convention of $2\pi\alpha' = 1$, the DBI action (4.14) for our D5-brane can be explicitly written as

$$S_{\mathrm{D5}} \sim \int dr dx \sqrt{r^2(1-\chi^2)\left(I_\chi + I_{A_t} + I_{\mathrm{mixed}}\right)}, \tag{4.15}$$

where we omit the factors of the integral that do not contribute to the field equations. The terms inside of the square-root of (4.15) are

$$I_\chi = r^2(1-\chi^2) + r^4 f(r)(\partial_r\chi)^2 + (\partial_x\chi)^2, \tag{4.16}$$

$$I_{A_t} = -(1-\chi^2)\left(r^2(\partial_r A_t)^2 + \frac{(\partial_x A_t)^2}{r^2 f(r)}\right), \tag{4.17}$$

$$I_{\mathrm{mixed}} = -\left(\partial_r\chi\partial_x A_t - \partial_x\chi\partial_r A_t\right)^2. \tag{4.18}$$

Using `Mathematica` to minimize the embedding surface action (4.15) with respect to the fields $\chi(r,x)$ and $A_t(r,x)$, we obtain two coupled second-order equations of motion. There are no Einstein equations to solve because of the fixed background metric. The exact form of our field equations are omitted here because of their length and cumbersomeness. We do note though that our action and field equation solutions agree with the findings of Refs [25, 26, 30, 31] and is of similar form to its D3-D7 analogue [29]. It is the inclusion of spatial dependence that complicates the field equations enough that numerical methods are needed to solve them.

4.4 Time-reversal invariance

The DBI action for our N_f D5 flavour probe branes in (4.14) is the DBI action of a single probe brane times by N_f. This set-up holographically realizes a Chern-Simons term of a level proportional to N_f, but this should not be mistaken as a $\mathbb{Z}$ classification because of the freedom of N_f as an integer. Rather, as mentioned in Ref [26], the even/odd parity of N_f is the $\mathbb{Z}_2$-valued quantity protected by time-reversal symmetry. The reasoning behind this is that the N_f pairs of massless fermions have a non-abelian $SU(2N_f)$ flavour symmetry group that transforms them non-trivially. It is always possible to turn on non-trivial components of the $SU(2N_f)$ group to create time-reversal invariant mass terms that add or subtract multiples of two from N_f such that the even/odd parity of the resulting N_f' is preserved. This shows how our holographic description is at least representing a time-reversal invariant system.[3] We set $N_f = 1$ for the remainder of our brane construction without any loss of generality.

4.5 Classes of D-brane embeddings

We take a moment now and classify what type of brane embeddings are possible in our set-up. At finite temperature, there are three distinct classes of D-brane embeddings that have been well studied and they are namely the Minkowski, critical, and black hole embeddings [30, 31, 50, 51, 55]. Each embedding class is defined by its behaviour near the black hole horizon which depends on the mass (controlled by θ), the chemical potential (controlled by A_t), and the temperature. Sketches of each embedding class are in Fig 4.3.

[3] Moreover in Refs [53, 54], the non-time-reversal invariant fields were projected out from the brane set-up and were found to give a $\mathbb{Z}_2$-valued D-brane charge.

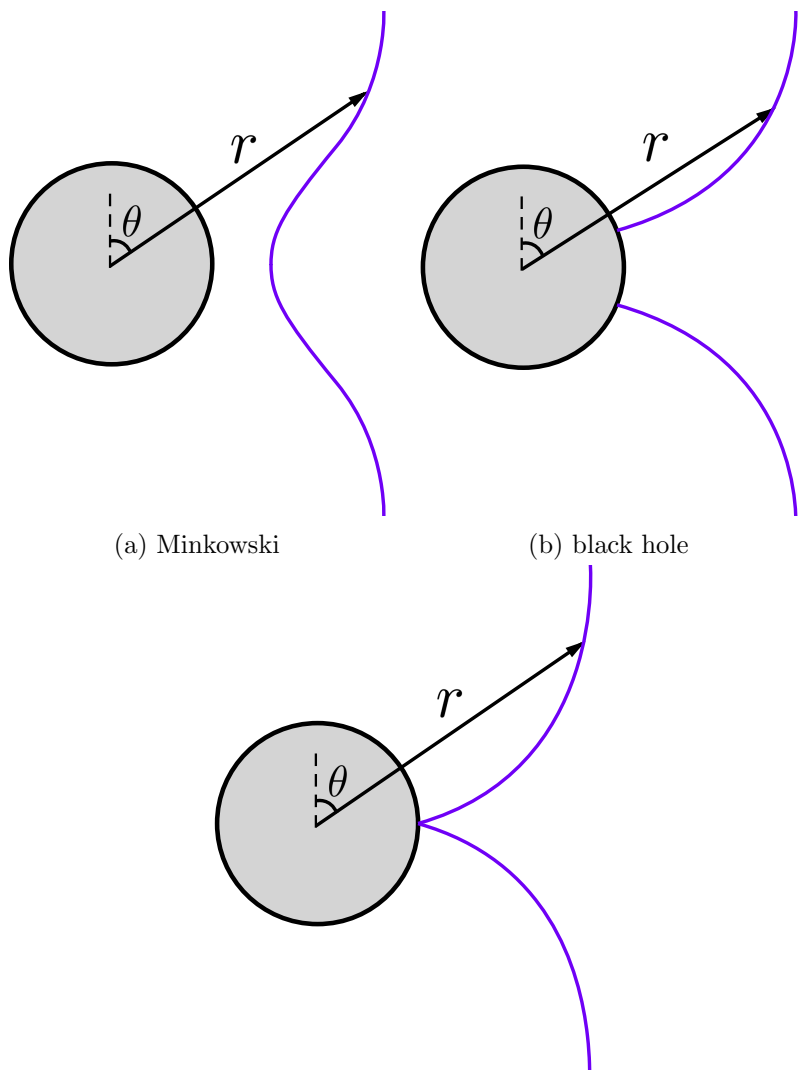

(a) Minkowski (b) black hole

(c) critical

Figure 4.3: Schematic diagrams of the Minkowski, critical, and black hole embeddings. The Minkowski embedding (Fig 4.3a) smoothly terminates outside of the black hole and forms a mass gap. Minkowski embeddings necessarily correspond to zero density states. The black hole embedding (Fig 4.3b) closes the mass gap by having the brane falling through the horizon. Black hole embeddings on the other hand can induce dense states. The critical embedding (Fig 4.3c) is the embedding intermediate to both the Minkowski and the black hole embedding where the brane just pinches off from the black hole. We focus mainly on black hole embeddings in this thesis.

Minkowski embeddings

Minkowski embeddings are the brane configurations where the probe D-brane does not reach the black hole horizon because either its surface tension is too strong or the gravitational pull of the black hole is too weak. The embedding ends smoothly at some finite distance $r_{\mathrm{D5}} > r_h$ outside of the event horizon leading to $\chi(r = r_{\mathrm{D5}}) = \pm 1$, or equivalently $\theta(r = r_{\mathrm{D5}}) = \pm\frac{\pi}{2}$, as seen in Fig 4.3a. Minkowski embeddings are gapped, exhibit a discrete mesonic spectrum, and necessarily correspond to states with zero density. If it was dense then it would imply electric field lines terminating abruptly between the D-brane and the black hole due to the physical separation. Minkowski embeddings are thermodynamically favoured at low temperatures with a low μ/M ratio. In the D3-D7 system, Minkowski embeddings are stable whenever the chemical potential satisfies $\mu < \mu_c = M$ at zero temperature.

Black hole embeddings

Black hole embeddings on the other hand are the embeddings that do reach the black hole horizon. These states are gapless, exhibit a continuous mesonic spectrum, and are typically dense. The probe D-brane acquires a value of $\chi(r = r_h) \in (-1, 1)$ at the horizon, or equivalently $\theta(r = r_h) \in \left(-\frac{\pi}{2}, \frac{\pi}{2}\right)$, as depicted in Fig 4.3b. For the types of black hole embeddings that we find, negative mass embeddings take on $\chi < 0$, positive mass embeddings take on $\chi > 0$, and zero mass embeddings take on $\chi = 0$ at the black hole horizon. Black hole embeddings are thermodynamically favoured at high temperatures or at least whenever the ratio μ/M is sufficiently high enough. A high chemical potential favours the black hole embedding because it fills the vacuum up with a Fermi sea of baryons to give density to the state. For the D3-D7 system, black hole embeddings can be achieved at zero temperature if the chemical potential satisfies $\mu > \mu_c = M$. The chemical potential threshold μ_c lowers with temperature for both the D3-D5 and D3-D7 systems as a result of thermal fluctuations assisting with the melting of mesons.

Critical embeddings

Critical embeddings are the configurations where the probe D-brane 'just' reaches the black hole horizon with $\chi(r = r_h) = \pm 1$, or equivalently $\theta(r = r_h) = \pm\frac{\pi}{2}$. They have zero density and are considered as the transitional

state between Minkowski and black hole embeddings. We do not consider them in this thesis.

4.6 Boundary conditions

In AdS/CFT, the physical observables of the strongly-coupled field theory are sourced in from the AdS boundary as boundary conditions, but these alone do not make up for all the boundary conditions – we also need regularity conditions. We require conditions for both $\chi(r,x)$ and $A_t(r,x)$ on each of the 4 boundaries of the two-dimensional $[r,x]$ grid and these one-dimensional boundaries are:

(B1) $r = [r_h, \infty)$ at negative spatial infinity $x = -\infty$

(B2) $r = [r_h, \infty)$ at positive spatial infinity $x = +\infty$

(B3) $x = (-\infty, +\infty)$ at the black hole horizon $r = r_h$

(B4) $x = (-\infty, +\infty)$ at radial infinity $r = \infty$

The simplest boundary conditions are on **(B1)** and **(B2)** – the spatial boundaries $x = \pm\infty$ that extend along the radial direction. We apply homogenous Neumann conditions to both fields, $\partial_x \chi = 0$ and $\partial_x A_t = 0$, on these boundaries. This boundary condition is not a strict choice but it is consistent with having a constant gauge field and mass profile spatially far away from the interface.

The boundary conditions on **(B3)** ensure the regularity of the field equations at the horizon $r = r_h$. At the horizon where $dt \to \infty$, we require A_t to vanish in order to keep $A_t dt$ as a well-defined 1-form gauge field with a finite norm [56, 57]. This is purely a physical condition; a near-horizon expansion of the field equations can only constrain the derivatives of A_t and not A_t itself. The horizon regularity condition on χ on the other hand can be derived by expanding the field equations at $r = r_h$ and doing so gives an embedding condition of $\partial_r \chi = \chi$.

Our final boundary conditions, which are on **(B4)**, feeds in the ultraviolet field theory from the AdS boundary. Generally one needs to cancel out the ultraviolet divergences of scalar quantities with the pertinent counterterms to ensure a finite partition function [58], but these results are already well known for many D3-Dq systems including ours so we simply state how our asymptotic fields match with the physical observables of the field theory dual [25, 50, 51, 59]. Expanding our field equations around $r = \infty$, the asymptotic behaviour of our two fields follow an ansatz of

$$\chi(r,x) = \frac{m(x)}{r} + \frac{c(x)}{r^2} + \ldots, \tag{4.19}$$

$$A_t(r,x) = \mu - \frac{n_b(x)}{r} + \ldots. \tag{4.20}$$

The holographic dictionary states that the leading term in our asymptotic expansion corresponds to a non-normalizable mode with an amplitude proportional to the coefficient of a gauge theory operator $\mathcal{O}$, and the sub-leading term corresponds to a normalizable mode with an amplitude proportional to the vacuum expectation of the operator $\langle\mathcal{O}\rangle$.[4]

For our embedding field χ, the dual operator is $\mathcal{O}_m$, the mass variation $\frac{\partial}{\partial m}$ of the super Yang-Mills Lagrangian. The leading term $m(x)$ as a result is proportional to the bare quark mass (or baryon mass). This quantity effectively describes the minimum length of the D3-D5 string. The sub-leading term $c(x)$ is assigned as the vacuum expectation $\langle\mathcal{O}_m\rangle$ which is proportional to the quark condensate.

For our gauge field A_t, the dual operator is $\mathcal{O}_q$, the quark charge density. The homogenous leading term μ is proportional to the chemical potential in the grand canonical ensemble. The sub-leading term $n_b(x)$ is matched with $\langle\mathcal{O}_q\rangle$ which is proportional to the quark number density (or baryon number density); this is a quantity related to the density of the D3-D5 strings pulling the D5-brane towards the black hole. We will use 'density' and 'number density' synonymously throughout this thesis.

The set of parameters $\{m(x), c(x)\}$ for χ are conjugate pairs, as with $\{\mu, n_b(x)\}$ for A_t. Solving the field equations with only one parameter of the conjugate pair specified at the boundary will fully determine the other conjugate variable as a 'response' from the bulk. We are free to choose which parameter of each conjugate pair to keep fixed, and therefore fix the chemical potential μ and the mass profile $m(x)$ so that $c(x)$ and $n_b(x)$ can be read off from the behaviour of χ and A_t at the boundary.[5] By inspection of ansatz (4.19) and (4.20), the total dimensionality of each conjugate pair is $2+1=3$ as expected from a (2+1)-dimensional Lagrangian [25].[6] The

[4] See the appendix of Ref [50] for more details.

[5] In Refs [25, 50, 51], a Legendre transformation was performed on the action to find the number density n_b to be a conserved quantity. This can reduce the spatially homogenous second-order field equation to first-order. Our spatially non-homogenous second-order field equations as far as we know do not allow for such a simplification unfortunately. Moreover, we find it more relevant to fix the chemical potential μ instead of n_b.

[6] The sub-leading terms $c(x)$ and $n_b(x)$ are of one less dimension in (2+1)D than they are in (3+1)D. The total dimensionality of the conjugate pairs adds up to 4 in (3+1)D.

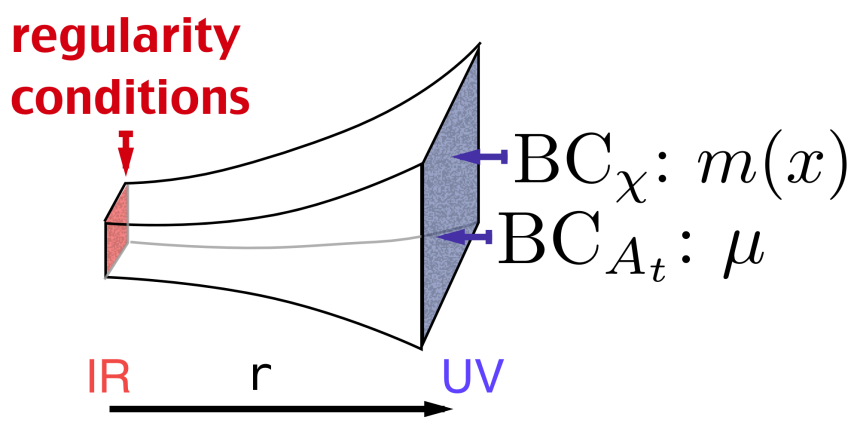

Figure 4.4: Boundary conditions on the horizon and boundary of the AdS$_5$ black hole. Not included here are the homogenous Neumann boundary conditions at the spatial boundaries $x = \pm\infty$. The horizon requires regularity conditions, and the boundary requires the specification of ultraviolet sources from the field theory. In our case, we feed in a mass profile $m(x)$ and a chemical potential μ into the bulk from the boundary.

final schematic of how our boundary conditions are imposed at $r = r_h$ and $r = \infty$ is shown in Fig 4.4.

4.7 Scaling symmetry

Our DBI action (4.15) enjoys scaling symmetry. It is crucial to identify all scaling symmetries from our problem to not only remove any redundancies, but to work in dimensionless parameters. We find the following scaling transformation

$$r \to ar, \qquad x \to x/a, \qquad \chi \to \chi, \qquad A_t \to A_t/a, \tag{4.21}$$

to be a scaling symmetry, and we make use of it by setting the radial horizon to unity so that our remaining physical degrees of freedom $\{m(x), \mu\}$ are in units of L, r_h, and α'. Our theory is now fully characterized by two dimensionless parameters

$$\tilde{m}(x) \equiv \frac{m(x)}{\pi T}, \qquad \tilde{\mu} \equiv \frac{\mu}{\pi T}, \tag{4.22}$$

which are namely the dimensionless quark mass profile $\tilde{m}(x)$, and the dimensionless chemical potential $\tilde{\mu}$. The dimensionless conjugate pairs to these variables are

$$\tilde{c}(x) \equiv \frac{c(x)}{(\pi T)^2}, \qquad \tilde{n}_b(x) \equiv \frac{n_b(x)}{(\pi T)^2}, \tag{4.23}$$

which are namely the dimensionless quark condensate $\tilde{c}(x)$, and the dimensionless quark density number $\tilde{n}_b(x)$. We will use tilde symbols to denote dimensionless variables in this thesis.

4.8 Realizing a holographic topological interface

Varying the mass $m(x)$ along the spatial direction x so that it discontinuously flips signs at $x = x_{\text{int}}$ will localize a domain wall at $x = x_{\text{int}}$. In practice, we have to interpolate $m(x)$ at $x = x_{\text{int}}$ with a steep but continuous function for the sake of numerical stability. We choose a mass profile $m(x)$ of the form

$$m(x) = \frac{2M}{1 + e^{-ax}} - M, \tag{4.24}$$

with a mass parameter $M > 0$, and a steepness parameter $a \gg 1$ chosen sufficiently high to approximate the sudden mass sign flip at $x = 0$. The mass profile takes on values $m(x) \approx M > 0$ (trivial insulator) when $x \gtrsim 0$, and $m(x) \approx -M < 0$ (non-trivial insulator) when $x \lesssim 0$. We find that our results are rather insensitive to the steepness parameter a, as it should be for sensible choices that are not too low nor too high.

A gapped system is naturally described by a Minkowski embedding, and a gapless one by a black hole embedding. Ideally one would like to sandwich a gapless system in between two distinct gapped phases by setting $\tilde{\mu} < \tilde{\mu}_c(\tilde{M})$ as shown in Fig 4.5a, but it is numerically difficult to incorporate both Minkowski and black hole embeddings together as one solution; it is much easier to implement a black hole embedding that extends through all values of x by increasing the chemical potential so that $\tilde{\mu} > \tilde{\mu}_c(\tilde{M})$ as shown in Fig 4.5b. The slight downside of this simplification is that it will unavoidably induce edge effects $\tilde{n}_b(x = \pm\infty) = \tilde{d} > 0$ outside of the interface as shown in Fig 4.6b, but the overall effect can be minimized by tuning $\tilde{\mu}$ to be closer but above $\tilde{\mu}_c(\tilde{M})$.

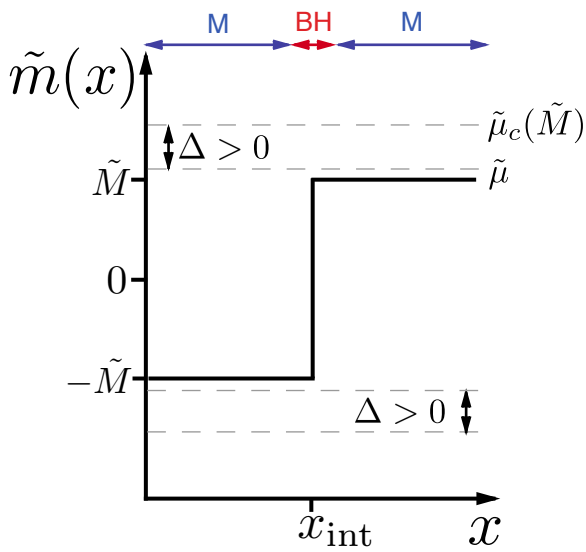

(a) An ideal $T > 0$ interface.

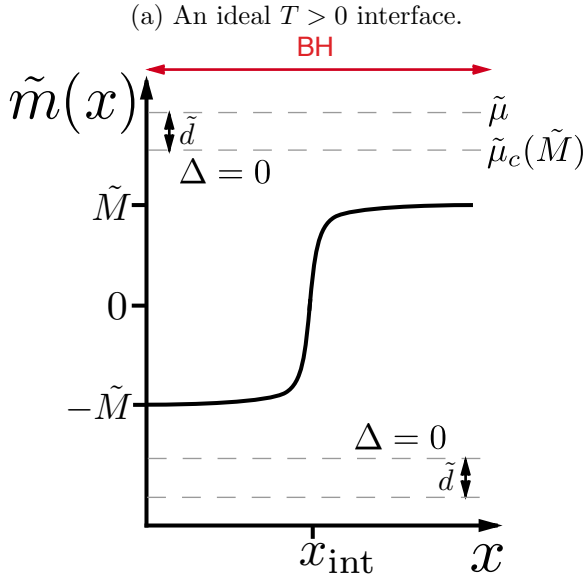

(b) Our $T > 0$ interface.

Figure 4.5: The ideal and our constructed mass profile $\tilde{m}(x)$ at finite temperature T. In the ideal profile (Fig 4.5a), we have a gapless interface at $x = 0$ sandwiched between two gapped insulators of differing topologies. It is realized with both Minkowski (M) and black hole (BH) embeddings. In our construction (Fig 4.5b), we consider a mass profile $\tilde{m}(x)$ that has a finite interface width and a chemical potential $\tilde{\mu} \gtrsim \tilde{\mu}_c(\tilde{M})$ that makes the embedding a black hole embedding for all x.

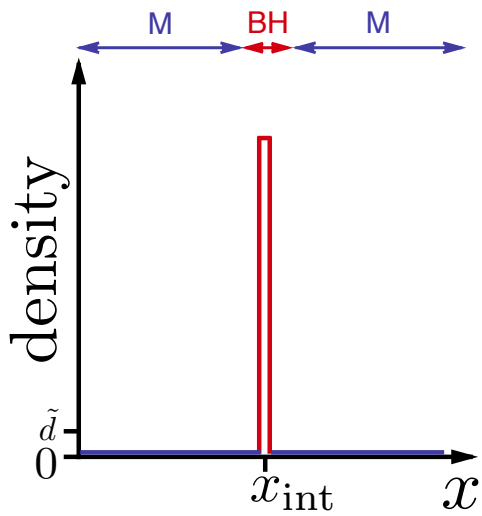

(a) An ideal $T \geq 0$ interface

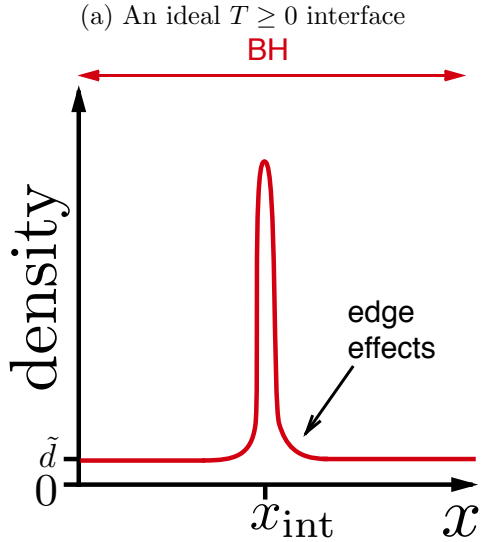

(b) Our $T > 0$ interface

Figure 4.6: A sketch of the quark density $n_b(x)$ as a function of the spatial direction x for the ideal and our constructed topological interface situated at $x = x_{\text{int}}$. A finite density $\tilde{d}$ is induced as a consequence of our construction but its effect can be reduced by keeping $\tilde{\mu} \gtrsim \tilde{\mu}(\tilde{M})$.

Chapter 5

Results and discussion

We solve our two field equations numerically on a two-dimensional Chebshev grid using spectral methods in `MATLAB` for dimensionless parameters $\tilde{\mu}$ and $\tilde{M}$.[7] The Chebyshev grid is prepared by compactifying the infinitely large $[r_{\min}, r_{\max}] \times [x_{\min}, x_{\max}] = [1, \infty) \times (-\infty, +\infty)$ grid with $z = 1/r$ and $y = \tanh(x)$ coordinate transformations. Chebyshev differentiation matrices are used to evolve the initial guess solution until convergence is met via the Newton-Raphson method. Our criteria for convergence requires both fields χ and $\tilde{A}_t$ to have a normalized residual error of less than 10^{-8}, and for this error to not change by more than 10^{-8} between the final two iterations.

We present first the results of the phase diagram for a spatially homogeneous mass profile $\tilde{m}(x) = \tilde{M}$. Afterwards, we implement the spatially non-homogenous mass profile $\tilde{m}(x) = \frac{2\tilde{M}}{1+e^{-ax}} - \tilde{M}$ from (4.24) and study the thermodynamics of a representative interface solution.

5.1 The phase diagram

The spatially homogenous topological insulator with mass $\tilde{M}$ can be studied by setting a flat mass profile $\tilde{m}(x) = M$. This is essentially the same as the one-dimensional case with no spatial dependence.[8] We present the $(\tilde{T}, \tilde{\mu}/\tilde{M})$ phase diagram in Fig 5.1 by maneuvering through the parameter space of black hole embeddings with dimensionless temperature $\tilde{T} \equiv \tilde{M}^{-1}$ and ratio $\tilde{\mu}/\tilde{M}$. We find the low $\tilde{T}$ solutions to be fairly sensitive to the initial guess solution so we obtain them by lowering the temperature adiabatically from high $\tilde{T}$ solutions.

The black hole embeddings with positive density $n_b > 0$ occupy the phase region above the black curve in Fig 5.1, this implicitly makes the phase region below the curve the $n_b = 0$ Minkowski embeddings. A chemical potential threshold $\tilde{\mu}_c = \tilde{\mu}_c(\tilde{T})$ must be overcome at low temperatures

[7] See Ref [60] for more details on implementing spectral methods in `MATLAB`.

[8] This is not exactly true because the boundary conditions at the horizon differ albeit slightly.

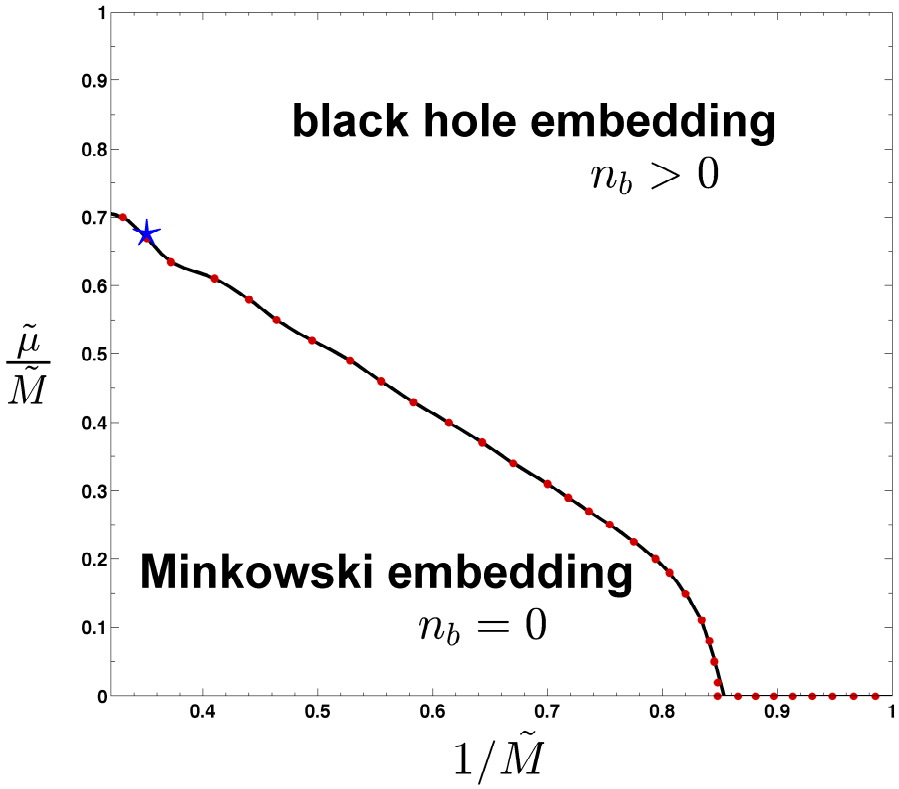

Figure 5.1: The homogenous ($\tilde{T} \equiv 1/\tilde{M}, \tilde{\mu}/\tilde{M}$) phase diagram. There are two types of embeddings: the $n_b > 0$ black hole embeddings and (implicitly) the $n_b = 0$ Minkowski embeddings. A chemical potential threshold $\tilde{\mu}_c > 0$ must be overcome at temperatures below $\tilde{T}_c \approx 0.87$ to favour the black hole embedding. However, above the critical temperature $\tilde{T}_c$, black hole embeddings are favoured regardless of how much chemical potential is fed in. The blue star on the left of the phase diagram are the parameters we use for our representative topological interface.

in order for black hole embeddings to be thermodynamically favoured – entropic excitations alone are not enough to pull the probe brane into the black hole. The chemical potential threshold ratio $\tilde{\mu}_c/\tilde{M}$ (the black curve) lowers as we raise the temperature and vanishes at a critical temperature $\tilde{T}_c \approx 0.87$; finite density black hole embeddings are stable past this critical temperature for any $\tilde{\mu} > 0$. The $(\tilde{T} > \tilde{T}_c, \tilde{\mu}/\tilde{M} = 0)$ line is where the black hole embeddings have zero density $n_b = 0$ and are in fact the high-temperature limits of the Minkowski embeddings.

There are strong qualitative similarities between the D3-D5 phase diagram and its D3-D7 counterpart [50, 61]. The high temperature phase transition between the Minkowski embedding and the black hole embedding is of first-order with discontinuous jumps in thermodynamical quantities *i.e.* the charge condensate and the entropic density. At low temperatures however, the system develops a critical point and the Minkowski/black hole phase transition disappears to allow for both phases to co-exist [25].

5.2 The holographic topological interface

Now we move on with a spatially non-homogenous mass profile $\tilde{m}(x) = \frac{2\tilde{M}}{1+e^{-ax}} - \tilde{M}$ to localize an interface at $x = 0$. The representative low temperature numerical solution we use takes on the dimensionless parameters $(\tilde{\mu} = 2.000, \tilde{M} = 2.954)$ as indicated by the blue star in Fig 5.1. The holographic interface was solved on a 40×40 Chebyshev grid and the $\chi(z, x)$ and $\tilde{A}_t(z, x)$ solutions are plotted in Fig 5.2 and Fig 5.3, respectively. The boundary behaviour is consistent with our previous analyses: Neumann boundary conditions $\partial_x \chi = \partial_x \tilde{A}_t = 0$ at the spatial infinities $x = \pm\infty$, $\chi \approx \tilde{m}(x)z + \tilde{c}(x)z^2$ and $\tilde{A}_t \approx \tilde{\mu} - \tilde{n}_b(x)z$ near the radial boundary $z = 0$, and $|\chi| < 1$ and $\tilde{A}_t \approx 0$ at the radial horizon $z = 1$.

The embedding field $\chi(z, x)$ in Fig 5.2 is an x-odd function, $\chi(z, x) = -\chi(z, -x)$, as with $\tilde{m}(x)$ about the interface. At each spatial point x, χ monotonically decreases in magnitude from the boundary to the horizon and has the same sign as $\tilde{m}(x)$. At $\tilde{m}(x) = 0$, the D5-brane splits the two topologies and is completely flat. The geometry of the brane embeddings can be visualized in isotropic coordinates as plotted in Fig 5.4. The D5-brane falls into the black hole horizon at all spatial points, with opposite mass sign embeddings doing so on opposite sides of the black hole about the $\chi = 0$ equator.

Our gauge field $\tilde{A}_t(z, x)$ solution in Fig 5.3 is rather simple to understand: chemical potential gets fed into the system from the boundary and the gauge

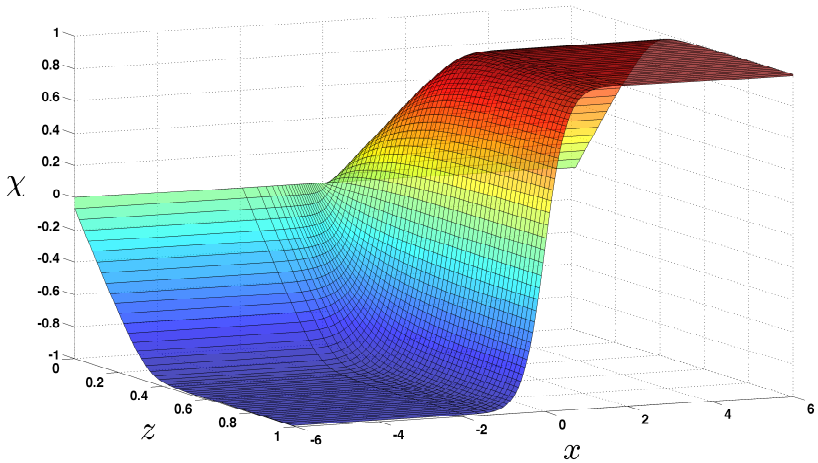

Figure 5.2: The numerical solution for $\chi(z,x)$ at low temperature $\tilde{T}(\tilde{\mu} = 2.000, \tilde{M} = 2.954) = 0.339$. The interface is at $x = 0$. The mass is positive for $x > 0$ (red curves in Fig 5.4), and negative for $x < 0$ (blue curves in Fig 5.4). The asymptotic behaviour goes as $\chi \approx \tilde{m}(x)z + \tilde{c}(x)z^2$ at the boundary and achieves an absolute value of less than one at the horizon.

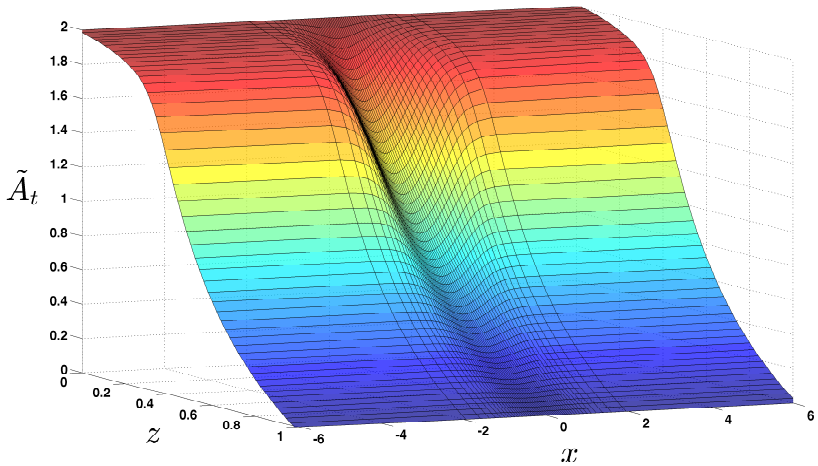

Figure 5.3: The numerical low temperature solution for $\tilde{A}_t(z,x)$ with $\tilde{T}(\tilde{\mu} = 2.000, \tilde{M} = 2.954) = 0.339$. The interface is at $x = 0$. The dip in the gauge field near $x = 0$ is a detection of higher density at the interface, which is most likely to be fermionic from our thermodynamic analyses. The asymptotic behaviour goes as $\tilde{A}_t \approx \tilde{\mu} - \tilde{n}_b(x)z$ at the boundary and vanishes at the horizon.

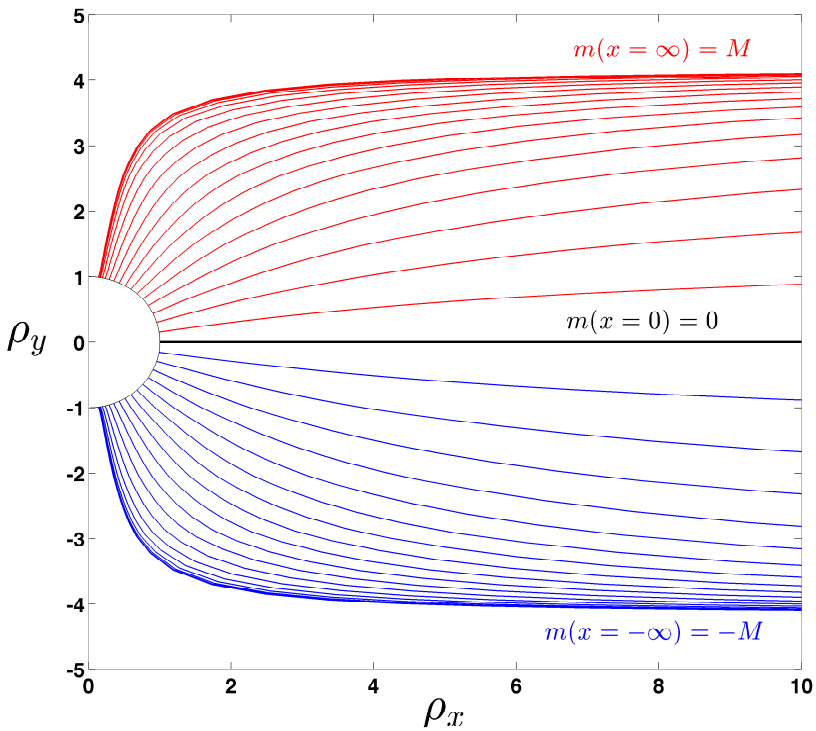

Figure 5.4: The probe D5-brane embeddings on the ρ_x-ρ_y plane where $\rho_x = \rho\cos\theta = \rho\sqrt{1-\chi^2}$, $\rho_y = \rho\sin\theta = \rho\chi$, and $\rho^2 = r^2 + \sqrt{r^4-1}$. Each curve represents a spatial grid point x with red, black, and blue curves corresponding to positive, zero, and negative mass black hole embeddings, respectively.

field monotonically decreases from $\tilde{\mu}$ to zero upon arrival at the horizon. We find also that the gauge field is x-even, $\tilde{A}_t(z,x) = \tilde{A}_t(z,-x)$, about the interface. Most interestingly there is a significant dip of $\tilde{A}_t$ at the interface provoked by the sub-leading term $\tilde{n}_b(x)$. The deeper the dipping of $\tilde{A}_t$ around $x = 0$, the more pronounced the interface density $\tilde{n}_b(x = 0)$ is relative to the background density $\tilde{n}_b(x \to \infty)$.

5.3 Thermal properties of the interface

The quark condensate $\tilde{c}(x)$ and density $\tilde{n}_b(x)$ can be read off as the sub-leading terms of χ and $\tilde{A}_t$ at the boundary – they are the bulk responses of fixing $\tilde{m}(x)$ and $\tilde{\mu}$ as sources. We fit third-order polynomials $p(x)_{\text{fit}} = p_0(x) + p_1(x)z + p_2(x)z^2 + p_3(x)z^3$ near the $z = 0$ boundary at each spatial grid point x, and collect the series coefficients $\tilde{c}(x) = p_2(x)_\chi$ for χ, and $\tilde{n}_b(x) = -p_1(x)_{\tilde{A}_t}$ for $\tilde{A}_t$.[9] The plots for our fitted $\tilde{c}(x)$ and $\tilde{n}_b(x)$ across the interface are given in Fig 5.5 and Fig 5.6, respectively.

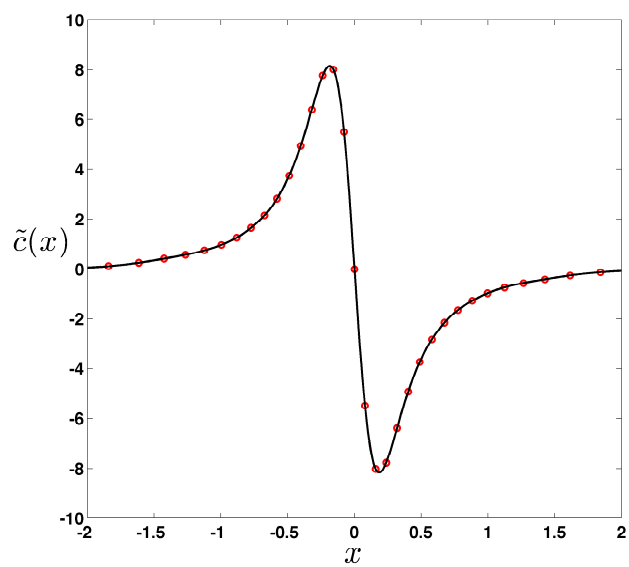

Figure 5.5: The condensate $\tilde{c}(x)$ across the $x = 0$ interface as a function of the spatial direction x. The red points are the actual spatial grid points, and the black curve interpolates between them.

[9] Sanity checks of $\tilde{m}(x) = p_1(x)_\chi$ and $\tilde{\mu} = p_0(x)_{\tilde{A}_t}$ were also made.

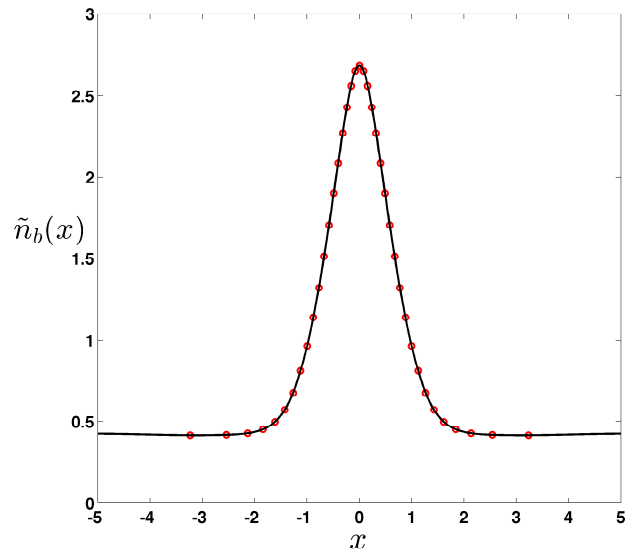

Figure 5.6: The quark density $\tilde{n}_b(x)$ across the $x = 0$ interface as a function of the spatial direction x. The red points are the actual spatial grid points, and the black curve interpolates between them.

Let us analyze the condensate $\tilde{c}(x)$ from Fig 5.5 first. Our x-odd mass profile makes $\tilde{c}(x)$ vanish at $x = 0$ by parity symmetry. Therefore chiral symmetry is preserved at the interface implying the existence of non-trivial fluid behaviour. Moreover we have chiral symmetry broken $\tilde{c}(x) \neq 0$ everywhere outside of $x = 0$. As with Ref [25], we find that $\tilde{c}(x)$ asymptotes to a small but finite constant at large masses. The large condensate peaks found near the vicinity of $x = 0$ are numerical artifacts of having an interface with finite width. What is important from the plot is that $\tilde{c}(x) = 0$ at the interface and $\tilde{c}(x) \neq 0$ everywhere else.

Just as $\tilde{A}_t$ is an x-even function, the quark density $\tilde{n}_b(x)$ from Fig 5.6 is also an x-even function with a density peak at $x = 0$. The density rises monotonically from the the spatial boundaries to the interface. The ratio of the interface density $\tilde{n}_b(x = 0)$ to the background density $\tilde{n}_b(x \to \pm\infty)$ can be increased by approaching the Minkowski/black hole transition at low temperatures; doing so lessens the significance of edge effects, but has the trade-off of being more computationally demanding because of the low temperature limit for a finite temperature problem.

More can be said about the interface by considering the interface density $\tilde{n}_b(x = 0)$ as a function of chemical potential. Due to our theory being fully characterized by the parameters $\tilde{\mu}$ and $\tilde{m}(x)$, the physics at the $\tilde{m} = 0$

interface will depend only on $\tilde{\mu}$. Therefore the leading-behaviour of the dimensionless free energy at the interface is restricted by dimensional analysis to be of the form $\tilde{\mathcal{F}} = \tilde{\mathcal{F}}(\tilde{\mu})$. For the fractional (3+1)D topological insulator studied in Ref [29], the leading behaviour of $\tilde{\mathcal{F}}$ at the interface was found to match with the free energy of non-interacting massless relativistic fermions $\tilde{\mathcal{F}}_{3+1}(\tilde{\mu}) \sim \tilde{\mu}^4$ at low temperatures [62]. We can expect our (2+1)D topological insulator by analogy to have an interface free energy scaling of one less dimension $\tilde{\mathcal{F}}_{2+1}(\tilde{\mu}) \sim \tilde{\mu}^3$, and thus a density scaling of $\tilde{n}_{b,2+1}(\tilde{\mu}) \sim \tilde{\mu}^2$ at low temperatures (high $\tilde{\mu}$). We plot in Fig 5.7 how our interface density scales as a function of chemical potential with $\tilde{M}$ set to some constant. The ansatz $\tilde{n}_b \sim \tilde{\mu}^\alpha$ is fitted at each $\tilde{\mu}$ by computing the scaling exponent $\alpha(\tilde{\mu}) = \frac{\partial}{\partial \log(\tilde{\mu})} \log(\tilde{n}_b(\tilde{\mu}))$. We find an $\alpha \approx 1.96$ plateau at high $\tilde{\mu}$, which is close to the theoretical $\alpha = 2$ scaling we would expect for free massless relativistic fermions.

Having α not being exactly equal to 2 at high $\tilde{\mu}$ suggests possible sub-leading contributions. These sub-leading contributions can reveal the nature of the interactions *i.e.* are they bosonic or fermionic? This is the essence of the hyperscaling violation exponent γ, it controls the scaling of the sub-leading terms in the number density by $\tilde{n}_b \sim \tilde{\mu}^2 + c_\gamma \tilde{\mu}^{2-\gamma}$ for constant c_γ. Degenerate fermions are assigned with $\gamma = 2$ and bosons with $\gamma = 0$. If the interface interactions are indeed Fermi surface like, then we would expect our density to scale by $\tilde{n}_b \sim \tilde{\mu}^2 + c_{\gamma=2}$ for non-zero $c_{\gamma=2}$ at high $\tilde{\mu}$. We fit $\tilde{n}_b \sim \tilde{\mu}^2 + c_{\gamma=2}$ to our data at high $\tilde{\mu}$ and find that $c_{\gamma=2}$ is in fact non-zero with more than 99% confidence to suggest that the interface interactions are fermionic.[10]

The last piece of evidence we present here is the fact that the interface is *almost* compressible [63]: it has translational invariance, a global $U(1)$ symmetry, and a density $\tilde{n}_b$ that is smooth with $\tilde{\mu}$. What is left to confirm compressibility is that these conditions remain true in the zero temperature ground state. In order for this to happen the global $U(1)$ gauge field must persist, and the system cannot break translational invariance by crystallizing. If this can be shown, we are guaranteed that our interface is a Fermi surface as a corollary of being compressible.

[10] Note that the bosonic hyperscaling violation exponent $\gamma = 0$ adds towards the overall leading behaviour of $\tilde{n}_b \sim \tilde{\mu}^2 + c_{\gamma=0}\tilde{\mu}^2 \sim \tilde{\mu}^2$, so the case of *purely* bosonic interactions is ignored in our analysis.

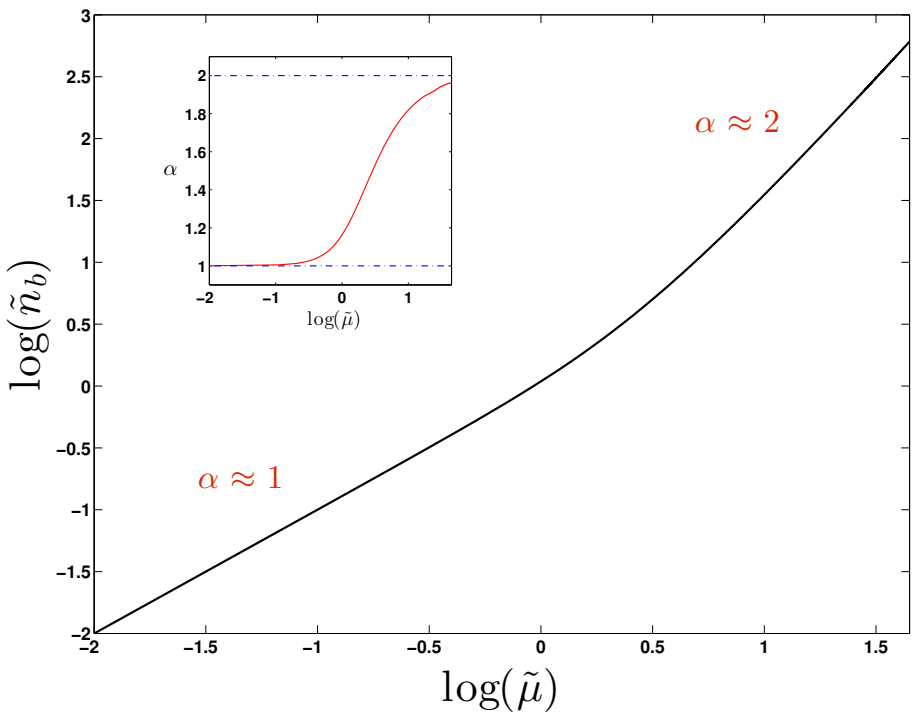

Figure 5.7: The scaling behaviour of the interface density, $\tilde{n}_b(x = 0)$, as a function of the chemical potential. The inset plot describes how the scaling exponent α from $\tilde{n}_b \sim \tilde{\mu}^\alpha$ varies with the chemical potential. At high temperatures (low $\tilde{\mu}$) the scaling goes as $\tilde{n}_b \sim \tilde{\mu}$, and at low temperatures (high $\tilde{\mu}$) the scaling goes as $\tilde{n}_b \sim \tilde{\mu}^2$.

Chapter 6

Conclusion

In this thesis, we realized the static holographic interface of a fractional (2+1)D time-reversal invariant topological insulator by embedding a D5 probe brane into (AdS_5 black hole) $\times S^5$ with a spatially non-homogenous mass profile $m(x)$ that switches signs at $x = 0$. The field equations were obtained by minimizing the DBI action of the embedding probe D5 brane with respect to the embedding parameter $\chi(r, x)$ and the $U(1)$ Maxwell gauge field $A_t(r, x)$, and these in turn were numerically solved using spectral methods on a two-dimensional Chebyshev grid. Our theory is fully characterized by two parameters: the dimensionless chemical potential $\tilde{\mu}$, and the dimensionless fermionic bulk mass $\tilde{M}$.

We considered first the spatially homogenous mass profile $\tilde{m}(x) = \tilde{M}$ and constructed its $(\tilde{T} \equiv 1/\tilde{M}, \tilde{\mu}/\tilde{M})$ phase diagram. Our D3-D5 phase diagram is qualitatively similar to its D3-D7 counterpart. Minkowski embeddings are thermodynamically favoured when the chemical potential $\tilde{\mu}$ is below a finite critical threshold $\tilde{\mu}_c$, but black hole embeddings are favoured once $\tilde{\mu}$ exceeds this threshold. At higher temperatures where $\tilde{T} > \tilde{T}_c \approx 0.87$, $\tilde{\mu}_c$ vanishes and finite density black hole embeddings are favoured for any given $\tilde{\mu} > 0$.

Next we studied the holographic topological interface of a representative low temperature phase point on our D3-D5 phase diagram close to the Minkowski/black hole phase transition. By applying the spatially non-homogenous mass profile $\tilde{m}(x) \equiv \frac{2\tilde{M}}{1+e^{-ax}} - \tilde{M}$ as a boundary condition and solving the corresponding field equations, we successfully realized a holographic topological interface. Furthermore we studied the thermodynamics of said interface by computing its $\tilde{n}_b(x = 0)$ scaling behaviour and found $\tilde{n}_b \sim \tilde{\mu}^2$ at high $\tilde{\mu}$ as expected of free massless relativistic electrons in (2+1) dimensions. The interface also exhibits a fermionic hyperscaling violation exponent. We can be guaranteed a Fermi surface by compressibility if the ground state preserves translational invariance, a global $U(1)$ gauge field, and a smooth density $\tilde{n}_b(\tilde{\mu})$.

Chapter 7

Prospective research

Holography can provide a qualitative phenomenological guide on what to look out for in strongly-interacting materials. We provide here some direct and indirect avenues of research to further our study on holographic topological insulators.

7.1 Zero temperature solution

Physically, the discreteness of the protected symmetries in topological insulators strongly suppresses small angle scattering at the boundary. Unfortunately the strength of this topological protection can get washed away by thermal fluctuations. The features of a degenerate Fermi gas are expected be sharper at zero temperature. Moving to zero temperature requires one to embed the D5-brane into $\mathrm{AdS}_5 \times S^5$ instead of (AdS_5 black hole) $\times S^5$ as we did so in this thesis. The difficulty with solving the corresponding zero temperature field equations comes from keeping the equations regular at the degenerate double pole horizon $r = 0$; it is simpler to deal with at finite temperature because the pole at the horizon $r = r_h > 0$ is non-degenerate. A zero temperature solution can also be used to confirm compressibility as discussed before. Computing the entanglement entropy and retarded Greens function of a zero temperature interface would also be interesting [64].

7.2 Integrating $n_b(x)$ over the interface

The density $n_b(x)$ represents a number density per unit area. Integrating $n_b(x)$ over the spatial x direction as $\int n_b(x)dx$ gives the density per unit length in the spatial y direction. Furthering our thermodynamical study by considering also the scaling behaviour of $\int n_b(x)dx$ as a function of μ is potentially significant experimentally. The difficulty in performing such a calculation lies in defining the spatial width of the interface $[x_{\min}, x_{\max}]$ because it is dynamically controlled by the interface width parameter $a \gg 1$ which we do not yet know the explicit dependence of. It would be useful

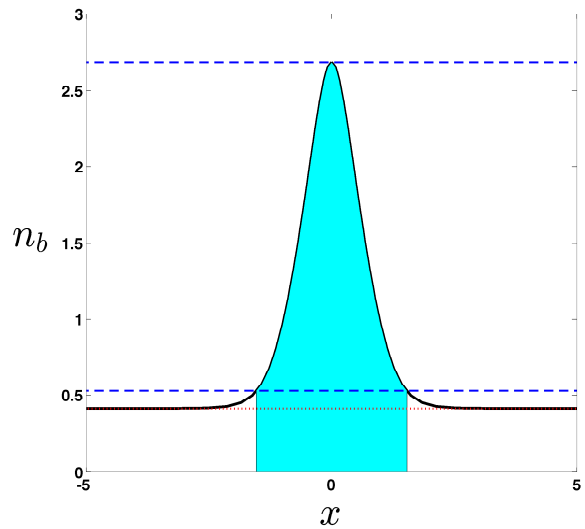

Figure 7.1: Our candidate interface width definition (cyan-filled area) on an $n_b(x)$ plot. The red dotted line represents the background density, and the blue dashed lines represent the density range of the interface width.

to know this dependence. Regardless, an example of a candidate interface width definition could be the maximum interval that satisfies

$$n_b(x) > n_{b,\text{background}} + 0.05\,(n_{b,\text{max}} - n_{b,\text{background}}) \tag{7.1}$$

everywhere in the interval. Here $n_{b,\text{max}} = n_b(x = 0)$ is the interface density and $n_{b,\text{background}} = n_b(x = \pm\infty)$ is the background density. This particular example defines the interface width as the maximum interval that has n_b above the background density plus 5% of the background-subtracted density peak $(n_{b,\text{max}} - n_{b,\text{background}})$. We illustrate this interface width definition in Fig 7.1.

7.3 Turning on an external magnetic field

Our D3-D5 system has a phase diagram that has been well studied in the presence of a constant external magnetic field [32, 65]. When the mass is zero, it is possible for a quantum phase transition to exist in the presence of an external magnetic field with the order parameter being the chiral condensate c. Turning up the magnetic field smoothly and studying how

it breaks away the topological protection of the interface states could be interesting.

7.4 Searching for the Majorana fermion

The Majorana fermion is a fermion which is its own antiparticle. They are suspected to be the unstable quasiparticles of topological superconductors. As topological superconductors have not yet been experimentally discovered, another possible way of finding the elusive Majorana fermion is by emulating the topological superconductor by placing a topological insulator in contact with a regular superconductor. What is hoped for is that the superconducting interface fermions can gain some sort of stability from the protective nature of the topological insulator. Constructing such a system holographically could provide experimentalists with useful methods for finding the elusive fermion.

Bibliography

[1] J. D. Bekenstein, "Black holes and entropy," *Phys. Rev. D*, vol. 7, pp. 2333–2346, Apr 1973.

[2] G. 't Hooft, "Dimensional Reduction in Quantum Gravity," *ArXiv General Relativity and Quantum Cosmology e-prints*, Oct. 1993.

[3] L. Susskind, "The world as a hologram," *Journal of Mathematical Physics*, vol. 36, pp. 6377–6396, Nov. 1995.

[4] J. Maldacena, "The Large-N Limit of Superconformal Field Theories and Supergravity," *International Journal of Theoretical Physics*, vol. 38, pp. 1113–1133, 1999.

[5] O. Aharony, S. S. Gubser, J. M. Maldacena, H. Ooguri, and Y. Oz, "Large N field theories, string theory and gravity," *Phys.Rept.*, vol. 323, pp. 183–386, 2000.

[6] A. Zaffaroni, "Introduction to the ads-cft correspondence," *Classical and Quantum Gravity*, vol. 17, no. 17, p. 3571, 2000.

[7] H. Nastase, "Introduction to AdS-CFT," *ArXiv e-prints*, Dec. 2007.

[8] A. V. Ramallo, "Introduction to the AdS/CFT correspondence," *ArXiv e-prints*, Oct. 2013.

[9] S. A. Hartnoll, C. P. Herzog, and G. T. Horowitz, "Holographic superconductors," *Journal of High Energy Physics*, vol. 12, p. 15, Dec. 2008.

[10] G. T. Horowitz, J. E. Santos, and B. Way, "Holographic josephson junctions," *Phys. Rev. Lett.*, vol. 106, p. 221601, Jun 2011.

[11] J. Erdmenger, C. Hoyos, A. O'Bannon, and J. Wu, "A Holographic Model of the Kondo Effect," *ArXiv e-prints*, Oct. 2013.

[12] T. Faulkner, N. Iqbal, H. Liu, J. McGreevy, and D. Vegh, "Holographic non-Fermi-liquid fixed points," *Royal Society of London Philosophical Transactions Series A*, vol. 369, pp. 1640–1669, Apr. 2011.

[13] L. Qing Fang, X.-H. Ge, and X.-M. Kuang, "Holographic fermions with running chemical potential and dipole coupling," *ArXiv e-prints*, Apr. 2013.

[14] J. L. Davis, P. Kraus, and A. Shah, "Gravity dual of a quantum Hall plateau transition," *Journal of High Energy Physics*, vol. 11, p. 20, Nov. 2008.

[15] M. Fujita, W. Li, S. Ryu, and T. Takayanagi, "Fractional quantum Hall effect via holography: Chern-Simons, edge states and hierarchy," *Journal of High Energy Physics*, vol. 6, p. 66, June 2009.

[16] O. Bergman, N. Jokela, G. Lifschytz, and M. Lippert, "Quantum Hall effect in a holographic model," *Journal of High Energy Physics*, vol. 10, p. 63, Oct. 2010.

[17] M. Rozali, D. Smyth, E. Sorkin, and J. B. Stang, "Holographic Stripes," *Physical Review Letters*, vol. 110, p. 201603, May 2013.

[18] L. Fu, C. L. Kane, and E. J. Mele, "Topological insulators in three dimensions," *Phys. Rev. Lett.*, vol. 98, p. 106803, Mar 2007.

[19] X.-L. Qi, T. L. Hughes, and S.-C. Zhang, "Topological field theory of time-reversal invariant insulators," *Phys. Rev. B*, vol. 78, p. 195424, Nov. 2008.

[20] M. Z. Hasan and C. L. Kane, "Colloquium: Topological insulators," *Reviews of Modern Physics*, vol. 82, pp. 3045–3067, Oct. 2010.

[21] X.-L. Qi and S.-C. Zhang, "The quantum spin Hall effect and topological insulators," *Physics Today*, vol. 63, no. 1, p. 010000, 2010.

[22] X.-L. Qi and S.-C. Zhang, "Topological insulators and superconductors," *Reviews of Modern Physics*, vol. 83, pp. 1057–1110, Oct. 2011.

[23] B. A. Bernevig and S.-C. Zhang, "Quantum Spin Hall Effect," *Physical Review Letters*, vol. 96, p. 106802, Mar. 2006.

[24] M. Levin and A. Stern, "Fractional Topological Insulators," *Physical Review Letters*, vol. 103, p. 196803, Nov. 2009.

[25] N. Evans and E. Threlfall, "R-Charge Chemical Potential in a 2+1 Dimensional System," *ArXiv e-prints*, July 2008.

[26] A. Karch, J. Maciejko, and T. Takayanagi, "Holographic fractional topological insulators in 2+1 and 1+1 dimensions," *Phys.Rev.*, vol. D82, p. 126003, 2010.

[27] M. C. Wapler, "Thermodynamics of holographic defects," *Journal of High Energy Physics*, vol. 1, p. 56, Jan. 2010.

[28] C. Hoyos-Badajoz, K. Jensen, and A. Karch, "A Holographic Fractional Topological Insulator," *Phys.Rev.*, vol. D82, p. 086001, 2010.

[29] M. Rozali, "Compressible Matter at an Holographic Interface," *Phys.Rev.Lett.*, vol. 109, p. 231601, 2012.

[30] A. Karch and A. O'Bannon, "Holographic thermodynamics at finite baryon density: some exact results," *Journal of High Energy Physics*, vol. 2007, no. 11, p. 074, 2007.

[31] M. Kulaxizi and A. Parnachev, "Remarks on Fermi liquid from holography," *Phys. Rev. D*, vol. 78, p. 086004, Oct. 2008.

[32] N. Evans, A. Gebauer, K.-Y. Kim, and M. Magou, "Phase diagram of the D3/D5 system in a magnetic field and a BKT transition," *Physics Letters B*, vol. 698, pp. 91–95, Mar. 2011.

[33] J. Dai, R. Leigh, and J. Polchinski, "New Connection Between String Theories," *Mod.Phys.Lett.A*, vol. 4, 1989.

[34] J. Polchinski, "Dirichlet branes and ramond-ramond charges," *Phys. Rev. Lett.*, vol. 75, pp. 4724–4727, Dec 1995.

[35] J. Polchinski, "TASI Lectures on D-Branes," *ArXiv High Energy Physics - Theory e-prints*, Nov. 1996.

[36] A. P. Schnyder, S. Ryu, A. Furusaki, and A. W. W. Ludwig, "Classification of topological insulators and superconductors in three spatial dimensions," *Phys. Rev. B*, vol. 78, p. 195125, Nov 2008.

[37] A. Kitaev, "Periodic table for topological insulators and superconductors," in *American Institute of Physics Conference Series* (V. Lebedev and M. Feigel'Man, eds.), vol. 1134 of *American Institute of Physics Conference Series*, pp. 22–30, May 2009.

[38] M. König, S. Wiedmann, C. Brüne, A. Roth, H. Buhmann, L. W. Molenkamp, X.-L. Qi, and S.-C. Zhang, "Quantum Spin Hall Insulator State in HgTe Quantum Wells," *Science*, vol. 318, pp. 766–, Nov. 2007.

[39] C. L. Kane, "Condensed matter: An insulator with a twist," *Nature Physics*, vol. 4, pp. 348–349, May 2008.

[40] C. Wu, B. A. Bernevig, and S.-C. Zhang, "Helical liquid and the edge of quantum spin hall systems," *Phys. Rev. Lett.*, vol. 96, p. 106401, Mar 2006.

[41] S. Murakami, "Two-dimensional topological insulators and their edge states," *Journal of Physics: Conference Series*, vol. 302, no. 1, p. 012019, 2011.

[42] B. Swingle, M. Barkeshli, J. McGreevy, and T. Senthil, "Correlated topological insulators and the fractional magnetoelectric effect," *Phys. Rev. B*, vol. 83, p. 195139, May 2011.

[43] O. Aharony, J. Pawełczyk, S. Theisen, and S. Yankielowicz, "Note on anomalies in the AdS-CFT correspondence," *Phys. Rev. D*, vol. 60, p. 066001, Sept. 1999.

[44] N. Seiberg *Phys. Lett. B*, vol. 206, 1988.

[45] A. Karch and L. Randall, "Open and closed string interpretation of SUSY CFT's on branes with boundaries," *Journal of High Energy Physics*, vol. 6, p. 63, June 2001.

[46] O. DeWolfe, D. Z. Freedman, and H. Ooguri, "Holography and defect conformal field theories," *Phys. Rev. D*, vol. 66, p. 025009, Jul 2002.

[47] J. Erdmenger, Z. Guralnik, and I. Kirsch, "Four-dimensional superconformal theories with interacting boundaries or defects," *Phys. Rev. D*, vol. 66, p. 025020, Jul 2002.

[48] A. Karch and E. Katz, "Adding flavor to AdS/CFT," *Journal of High Energy Physics*, vol. 6, p. 43, June 2002.

[49] J. Erdmenger, N. Evans, I. Kirsch, and E. J. Threlfall, "Mesons in gauge/gravity duals," *European Physical Journal A*, vol. 35, pp. 81–133, Jan. 2008.

[50] S. Kobayashi, D. Mateos, S. Matsuura, R. C. Myers, and R. M. Thomson, "Holographic phase transitions at finite baryon density," *Journal of High Energy Physics*, vol. 2007, no. 02, p. 016, 2007.

[51] D. Mateos, R. C. Myers, and R. M. Thomson, "Holographic Phase Transitions with Fundamental Matter," *Physical Review Letters*, vol. 97, p. 091601, Sept. 2006.

[52] G. V. Dunne, "Course 3: Aspects of Chern-Simons Theory," in *Topological Aspects of Low Dimensional Systems* (A. Comtet, T. Jolicoeur, S. Ouvry, and F. David, eds.), p. 177, 1999.

[53] S. Ryu and T. Takayanagi, "Topological insulators and superconductors from D-brane," *Physics Letters B*, vol. 693, pp. 175–179, Sept. 2010.

[54] S. Ryu and T. Takayanagi, "Topological insulators and superconductors from string theory," *Phys. Rev. D*, vol. 82, p. 086014, Oct. 2010.

[55] V. P. Frolov, "Merger transitions in brane black-hole systems: Criticality, scaling, and self-similarity," *Phys. Rev. D*, vol. 74, p. 044006, Aug. 2006.

[56] S. S. Gubser, "Breaking an abelian gauge symmetry near a black hole horizon," *Phys. Rev. D*, vol. 78, p. 065034, Sep 2008.

[57] S. S. Gubser, "Colorful horizons with charge in anti-de sitter space," *Phys. Rev. Lett.*, vol. 101, p. 191601, Nov 2008.

[58] K. Skenderis, "Lecture Notes on Holographic Renormalization," *ArXiv High Energy Physics - Theory e-prints*, Sept. 2002.

[59] A. Karch, A. O'Bannon, and K. Skenderis, "Holographic renormalization of probe D-branes in AdS/CFT," *Journal of High Energy Physics*, vol. 4, p. 15, Apr. 2006.

[60] L. Trefethen, *Spectral Methods in MATLAB*. Society for Industrial Mathematics, Philadelphia, 2000.

[61] D. Mateos, S. Matsuura, R. C. Myers, and R. M. Thomson, "Holographic phase transitions at finite chemical potential," *Journal of High Energy Physics*, vol. 11, p. 85, Nov. 2007.

[62] L. Homorodean, "Thermal properties of degenerate relativistic quantum gases," *Modern Physics Letters B*, vol. 17, no. 18, pp. 991–1010, 2003.

[63] L. Huijse, S. Sachdev, and B. Swingle, "Hidden Fermi surfaces in compressible states of gauge-gravity duality," *Phys. Rev. B*, vol. 85, p. 035121, Jan. 2012.

[64] B. Swingle, L. Huijse, and S. Sachdev, "Entanglement entropy of compressible holographic matter: loop corrections from bulk fermions," *ArXiv e-prints*, Aug. 2013.

[65] K. Jensen, A. Karch, D. T. Son, and E. G. Thompson, "Holographic Berezinskii-Kosterlitz-Thouless Transitions," *Physical Review Letters*, vol. 105, p. 041601, July 2010.

Appendix A

Chern-Simons terms of the integer QSH state

It is only in (2+1)-dimensions that Chern-Simons theory is quadratic in the gauge field. The $A^a \wedge dA^b$ Chern-Simons terms in our theory has a Chern-Simons term of level

$$k = \frac{1}{2}\sum_i q_i^{\mathrm{a}} q_i^{\mathrm{b}} \mathrm{sgn}(m_i), \tag{A.1}$$

where the index i runs through all the fermionic fields, the latin indices a, b run through our two $U(1)$ Maxwell and R symmetries, q is the fermionic charge, and $\mathrm{sgn}(m_i)$ is the sign of the fermionic mass. The Maxwell and R charges can take values of either ± 1. There are in general $q_i^{\mathrm{Maxwell}} q_i^{\mathrm{Maxwell}}$ and $q_i^R q_i^R$ contributions to the summation of (A.1) associated with the $A^{\mathrm{Maxwell}} \wedge dA^{\mathrm{Maxwell}}$ and $A^R \wedge dA^R$ Chern-Simons terms, but these positive charge-squared $(q^a)^2 = 1$ terms get cancelled out from the calculation because the fermion pairs have oppositely-signed masses. Be that as it may the $A^R \wedge dA^{\mathrm{Maxwell}}$ Chern-Simons term is the mixed term that remains non-zero because even though the Maxwell charges of a fermion pair are the same, both the R-charges and masses are of opposite signs. This leads to the integer QSH effect with an anomalous Chern-Simons term of level

$$k = \frac{1}{2}\sum_i q_i^{\mathrm{Maxwell}} q_i^R \mathrm{sgn}(m_i) \tag{A.2}$$

$$= \mathrm{sgn}(m) N_f. \tag{A.3}$$

These arguments are directly transferrable to the fractional case with the only difference being the magnitude of the charges.

Appendix B

Calculation of the AdS black hole Hawking temperature

The simplest and most typical way of calculating the Hawking temperature of the AdS black hole is by Euclideanizing it and removing the conical singularity at the horizon by identifying the period of $\tau = it$ with its inverse temperature $\beta = T^{-1}$. Physically, what this does is it implicitly matches the trace of the Euclideanized quantum mechanical evolution operator $e^{-\tau\mathcal{H}}$ with the thermodynamic partition function $\mathcal{Z} = \mathrm{tr}\left[e^{-\beta\mathcal{H}}\right]$. Starting with the AdS_5 black hole metric

$$ds^2 = -\frac{r^2}{L^2}f(r)dt^2 + \frac{L^2}{r^2}\frac{dr^2}{f(r)} + \frac{r^2}{L^2}d\vec{x}_3^2, \tag{B.1}$$

$$f(r) = 1 - \frac{r_h^4}{r^4}, \tag{B.2}$$

we Wick rotate the metric with $\tau = it$ and expand it just outside of the horizon $r = r_h + \epsilon$ to get

$$ds^2 \approx \frac{4r_h\epsilon}{L^2}d\tau^2 + \frac{L^2}{4r_h\epsilon}d\epsilon^2 + \frac{r^2}{L^2}d\vec{x}_3^2 \tag{B.3}$$

from $r^2 f(r) \approx 4r_h\epsilon + \mathcal{O}(\epsilon^2)$ near the horizon. To realize the conical singularity explicitly, we move into spherical coordinates using transformations $\rho^2 = \frac{\epsilon L^2}{r_h}$ and $\chi = \frac{2r_h\tau}{L^2}$ to get the first two components of our metric (radial and temporal) to be

$$ds_2^2 = \rho^2 d\chi^2 + d\rho^2. \tag{B.4}$$

Eliminating the conical singularity requires χ to have a period of 2π and thus requires τ to have a period of $\frac{\pi L^2}{r_h}$. Matching this with β gives a Hawking temperature of

$$T \equiv \beta^{-1} = \frac{r_h}{\pi L^2}. \tag{B.5}$$